

# Azetidines Kill Multidrug-Resistant *Mycobacterium tuberculosis* without Detectable Resistance by Blocking Mycolate Assembly

Yixin Cui, Alice Lanne, Xudan Peng, Edward Browne, Apoorva Bhatt, Nicholas J. Coltman, Philip Craven, Liam R. Cox, Nicholas J. Cundy, Katie Dale, Antonio Feula, Jon Frampton, Martin Fung, Michael Morton, Aaron Goff, Mariwan Salih, Xingfen Lang, Xingjian Li, Chris Moon, Jordan Pascoe, Vanessa Portman, Cara Press, Timothy Schulz-Utermoehl, Suki Lee, Micky D. Tortorella, Zhengchao Tu, Zoe E. Underwood, Changwei Wang, Akina Yoshizawa, Tianyu Zhang, Simon J. Waddell, Joanna Bacon, Luke Alderwick,\* John S. Fossey,\* and Cleopatra Neagoie\*



Cite This: <https://doi.org/10.1021/acs.jmedchem.3c01643>



Read Online

ACCESS |



Metrics & More

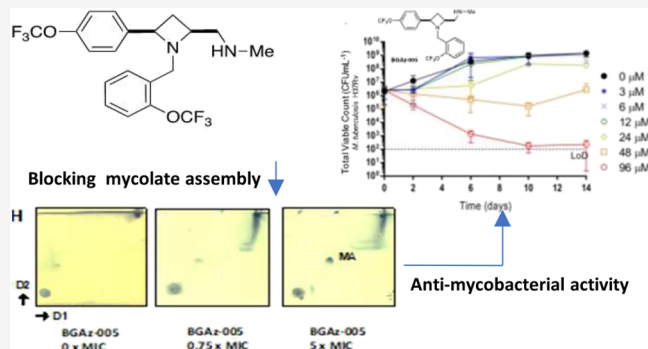


Article Recommendations



Supporting Information

**ABSTRACT:** Tuberculosis (TB) is the leading cause of global morbidity and mortality resulting from infectious disease, with over 10.6 million new cases and 1.4 million deaths in 2021. This global emergency is exacerbated by the emergence of multidrug-resistant MDR-TB and extensively drug-resistant XDR-TB; therefore, new drugs and new drug targets are urgently required. From a whole cell phenotypic screen, a series of azetidines derivatives termed BGaz, which elicit potent bactericidal activity with MIC<sub>99</sub> values <10  $\mu$ M against drug-sensitive *Mycobacterium tuberculosis* and MDR-TB, were identified. These compounds demonstrate no detectable drug resistance. The mode of action and target deconvolution studies suggest that these compounds inhibit mycobacterial growth by interfering with cell envelope biogenesis, specifically late-stage mycolic acid biosynthesis. Transcriptomic analysis demonstrates that the BGaz compounds tested display a mode of action distinct from the existing mycobacterial cell wall inhibitors. In addition, the compounds tested exhibit toxicological and PK/PD profiles that pave the way for their development as antitubercular chemotherapies.



## INTRODUCTION

Tuberculosis (TB) is the principal infectious disease and cause of death worldwide, accounting for 1.4 million deaths in 2021. One-third of the world's population is currently infected with latent TB, and over 10 million new cases of active TB are recognized per annum.<sup>1,2</sup> Patients suffering from TB are treated with a cocktail of four drugs over a 6-month period. While cure rates can be as high as 90–95%,<sup>3</sup> a combination of poor patient compliance and pharmacokinetic variability has led to the emergence of multidrug-resistant (MDR) and extensively drug-resistant (XDR) TB.<sup>4,5</sup> The alarming increase in MDR-TB (500,000 new cases in 2018),<sup>1</sup> coupled with the fact that the last novel frontline anti-TB drug, rifampicin, was discovered over 40 years ago,<sup>6</sup> suggests that development and implementation of new control measures are essential for the future abatement of TB.<sup>7,8</sup> Herein, the identity and antimycobacterial activity of azetidine derivatives with MIC<sub>99</sub> values <10  $\mu$ M against *Mycobacterium tuberculosis* are disclosed. These compounds did not give rise to emerging specific resistance in mycobacterial model organism *Mycobacterium smegmatis* and *Mycobacterium bovis* BCG. The mode of action

and target deconvolution studies suggest that mycobacterial growth inhibition is conferred by a hitherto uncharacterized mechanism that arrests late-stage mycolic acid biosynthesis. DMPK and toxicology profiles confirm that the azetidine derivatives identified display relevant and acceptable profiles for translation.

## RESULTS

**Identification and Development of Azetidine Derivatives with Antimycobacterial Activity.** A bespoke compound library of novel lead-like small molecules<sup>9</sup> for activity screening, which displayed a high fraction of sp<sup>3</sup> (Fsp<sup>3</sup>, an indication of complexity and 3D-character)<sup>10–12</sup> atoms, were free from pan-assay interference compounds

**Received:** September 5, 2023

**Revised:** December 19, 2023

**Accepted:** January 23, 2024

Table 1. Activity-guided SAR Expansion of Hit Azetidine BGaz-001-016<sup>a,b</sup>

Entry	Compound	Structure	<i>M. smeg.</i> MIC <sub>99</sub> (μM) <sup>(a)</sup>	BCG MIC <sub>99</sub> (μM) <sup>(a)</sup>	Mol. wt (g/mol)	log P	TPSA (Å <sup>2</sup> )	Fsp <sup>3</sup>
1	BGAz-001		30.5	65	385.349	4.84	6.48	0.43
2	BGAz-002		32	15	474.447	6.93	24.94	0.48
3	BGAz-003		26	22	521.345	6.6	6.48	0.48
4	BGAz-004		14	14	543.141	6.38	6.48	0.43
5	BGAz-005		24	21	434.382	6.14	33.73	0.4
6	BGAz-006		14	11	454.23	6.05	6.48	0.43
7	BGAz-007		23	24	457.335	6.26	24.5	0.43
8	BGAz-008		23	26	462.436	6.92	33.73	0.45
9	BGAz-009		29	30	478.435	6.1	42.96	0.45
10	BGAz-010		100	42.6	415.375	4.68	15.71	0.45
11	BGAz-011		87	45	378.439	5.49	24.5	0.43
12	BGAz-012		80	48	517.103	5.97	6.48	0.37
13	BGAz-013		94	51	373.338	4.82	15.27	0.40
14	BGAz-014		100	54	527.098	5.82	15.27	0.30
15	BGAz-015		100	56	559.471	8.14	15.71	0.38
16	BGAz-016		100	60	543.472	7.58	6.48	0.38

<sup>a</sup>MIC<sub>99</sub> as determined by a modified Gompertz function. <sup>b</sup>MIC values were determined from three biological replicates using a resazurin end point assay.

(PAINS),<sup>13,14</sup> and are synthetically tractable, allowing for hit-to-lead scaffold elaboration,<sup>15</sup> were sought. Unrelated synthetic chemistry methodology studies<sup>16</sup> proved to be an ideal untapped source of such compounds.<sup>17–20</sup> Compounds were fed into an open-ended antimycobacterial compound screen at the University of Birmingham Drug Discovery Facility.<sup>21</sup> From that, an azetidine derivative **BGAz-001** (Table 1, entry 1), which displayed promising antimycobacterial activity against both *Mycobacterium smegmatis* and *Mycobacterium bovis* BCG, with MICs of 30.5 and 64.5  $\mu$ M, respectively, was identified, and further azetidine derivatives were synthesized at Guangzhou Institutes of Biomedical Health (GIBH).<sup>22</sup> Preliminary compound screening at 2 and 20  $\mu$ M in an end point REMA assay to assess antimycobacterial activity, with subsequent secondary MIC determination against BCG and *M. smegmatis* (MIC refers to MIC<sub>99</sub> unless otherwise stated), was sufficient to rule out the majority of ancillary compounds for further study.<sup>23</sup> Analogues of the best performing compounds were synthesized, and structure–activity relationship (SAR) investigation was undertaken. Based on the screening results, 16 azetidine derivatives with MIC values against *M. smeg.* strains or *M. bovis* BCG strains lower than 100  $\mu$ M are listed in Table 1. Ten of these molecules had a molecular weight less than 500 Da, and 14 had cLogP values lower than 7, indicating an overall good potential for further anti-TB drug discovery based on their physicochemical property aspects.

Compared with **BGAz-001**,  $R^1$  = phenyl (Figure 1), the compounds containing the electron-withdrawing group-

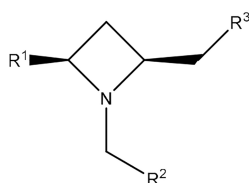


Figure 1. BGAz derivatives synthesized.

functionalized phenyl ring of  $R^1$  (**BGAz-003**, **BGAz-004**, and **BGAz-006**) showed greatly increased activities against both *M. bovis* BCG and *M. smeg.* organisms, while **BGAz-002** showed similar activity against *M. smeg.* and better activity against *M. bovis* BCG (Table 1). It clearly appears that the electron-withdrawing group-functionalized phenyl ring of  $R^1$  favored inhibition against *M. smeg.* and *M. bovis* BCG compared with analogues decorated with an electron-donating group-functionalized phenyl ring of  $R^1$ , (**BGAz-010**, Table 1). Introduction of electron-withdrawing groups ( $-\text{Br}$ ,  $-\text{Cl}$ ,  $-\text{CF}_3$ , and  $-\text{OCF}_3$ ) at the *para* and *meta* positions of the pendant aryl rings  $R^1$  resulted in an approximately three- to four-fold increase in activity against *M. bovis* BCG (**BGAz-002**, **BGAz-003**, and **BGAz-004**) or six-fold increase (**BGAz-006**) when compared to **BGAz-001**. Among the BGAz derivatives synthesized, active compounds often contained either a bromo substituent or trifluoromethyl ether at the *ortho* position of the azetidine *N*-benzyl group ( $R^2$ , Figure 1) provided by this methodology. Regarding the  $R^3$ , the amine pendant group (Figure 1), replacing the pyrrolidine with a methyl-, isopropyl-, or methoxypropyl-amine, while phenyl ring  $R^1$  bears an electron-withdrawing group, results in compounds (**BGAz-005**, **BGAz-007**, **BGAz-008**, and **BGAz-009** respectively), which retain antimycobacterial activity, with an approximately

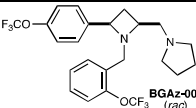
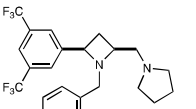
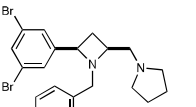
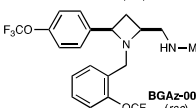
three-fold increase in activity against *M. bovis* BCG (**BGAz-005**) or with an approximately two-fold increase against *M. bovis* BCG (**BGAz-007**, **BGAz-008**, and **BGAz-009**). The inhibition against both *M. smeg.* and *M. bovis* BCG was considerably reduced when the pendant amine was dimethylamine and propargylamine, **BGAz-012** and **BGAz-014** (Table 1). Further iterations of BGAz modification included permutations of the pendant amines (isopropylamine), and aryl ring combinations ( $R^1$  = phenyl and  $R^2$  = trifluoromethoxyphenyl, bromomethyl) resulted in compounds with marginally reduced antimycobacterial activity (**BGAz-011** and **BGAz-013**), showing the importance of the electron-withdrawing group-functionalized phenyl ring  $R^1$ . In addition, the inclusion of piperidine derivatives as pendant amines provided no further enhancement in antimycobacterial activity (**BGAz-015** – **BGAz-016**).

Therefore, four azetidine-analogues (**BGAz-002** – **BGAz-005**) with satisfactory activity against model organisms, which were representative of the subclass of chemistry identified, were selected for further evaluation. Compared with **BGAz-007**, **BGAz-008**, and **BGAz-009**, **BGAz-005** showed similar MIC values against *M. smeg.* but lower MIC values against *M. bovis* BCG. **BGAz-006** with the lowest MIC values was also encouraging for further development; however, due to time limitations, this was not included in this project. Antitubercular activity of azetidine derivatives (**BGAz-002**–**BGAz-005**) was observed.

Compounds **BGAz-002**–**BGAz-005** displayed antitubercular activity against *M. tuberculosis* strains that include reference strains H37Ra::pTYOK and H37Rv, and two clinical isolates *M. tuberculosis* (Beijing/W lineage 1192/015) and *M. tuberculosis* (Beijing 08/00483E) that are drug-sensitive or multi-drug-resistant to isoniazid, rifampicin, pyrazinamide, and ethambutol (Table 2).

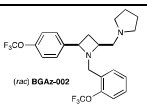
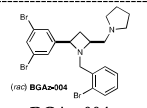
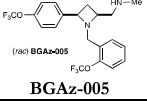
Compounds **BGAz-002**–**BGAz-005** elicited antitubercular activities ranging from 4.5–9.2  $\mu$ M MIC<sub>lux50</sub> using a recently reported autoluminescent avirulent strain of *M. tuberculosis* H37Ra (Table 2, entries 1–4). Both **BGAz-003** and **BGAz-004** inhibit *M. tuberculosis* (H37Rv) at an MIC of 3.3  $\mu$ M (Table 2, entries 2 and 3), with **BGAz-002** and **BGAz-005** inhibiting growth at MICs of 6.2 and 7.2  $\mu$ M, respectively (Table 2, entries 1 and 4). The MICs determined for **BGAz-002**–**BGAz-005** are higher in the drug-sensitive *M. tuberculosis* Beijing/W (1192/015) clinical isolate compared to H37Rv. When comparing MICs between drug-sensitive and drug MDR clinical strains, no significant differences were observed for **BGAz-002**–**BGAz-004**, suggesting that the acquisition of mutations conferring front-line drug resistance does not impact the antitubercular activity of these compounds. However, it is noteworthy that **BGAz-005** was tested against *M. tuberculosis* 08/00483E, which is a clinical isolate that was sequenced at PHE (UKHSA) Porton using whole genome sequencing. The strain was confirmed to be resistant to all four frontline drugs (isoniazid, rifampicin, pyrazinamide, and ethambutol), as it has the following mutations, *katG* S315, *rpoB*, S450, *pncA*+T186, and *embB* M306 V.<sup>25</sup> **BGAz-005** displayed an 8-fold lower MIC (2.8  $\mu$ M, Table 2, entry 4) in comparison to the drug-sensitive isolate. The absence of cross-resistance of these new anti-TB agents with the current frontline TB drugs is an important consideration in the development of new TB therapies with distinct modes of action.<sup>26</sup> Evaluation of the minimal bactericidal concentrations (MBCs) for **BGAz-002**–**BGAz-005** against BCG demonstrates that these compounds

Table 2. MIC and MBC Values of the BGaz-002–BGaz-005 against Mycobacterial Strains With Different Drug-susceptibility Profiles<sup>a</sup>

Entry	Compound	BCG MBC ( $\mu$ M)	<i>M. tb</i> H37Ra::pTY OK MIC <sub>lux50</sub> ( $\mu$ M)	<i>M. tb</i> H37Rv MIC <sub>99</sub> ( $\mu$ M) ( <sup>a</sup> )	<i>M. tb</i> 1192/015 MIC <sub>99</sub> ( $\mu$ M) ( <sup>a</sup> )	<i>MDR-M. tb</i> 08/00483E MIC <sub>99</sub> ( $\mu$ M) ( <sup>a</sup> )
1	 BGaz-002 (rac)	12–25	9.2	6.2	37.8	33.5
2	 BGaz-003 (rac)	12–25	6.9	3.3	19.1	16.8
3	 BGaz-004 (rac)	12–25	7.03	3.3	15.4	15.6
4	 BGaz-005 (rac)	12–25	4.5	7.2	23.2	2.8

<sup>a</sup>The *M. tb* H37Ra::pTYOK is an auto-luminescent strain of mycobacteria.<sup>24</sup> The MIC<sub>99</sub> values of BGaz-002–BGaz-005 against *M. smegmatis* and *M. bovis* BCG, drug-sensitive *M. tuberculosis* H37Rv (reference strain) and *M. tuberculosis* 1192/015 (clinical isolate), and multi-drug-resistant *M. tuberculosis* 08/00483E (clinical isolate resistant to INH, RIF, PZA and EMB). MIC values were determined from three biological replicates using a resazurin end point assay. The minimum bactericidal concentration (MBC) was determined for BGaz-002–BGaz-005 against *M. bovis* BCG.

Table 3. Pharmacokinetic Profiles, CYP450 Activities, Mitochondrial Dysfunction, and hERG Liabilities of BGaz-002, BGaz-004, and BGaz-005

Entry	Compound	Dose (mg /kg)	C <sub>max</sub> (Mouse, P.O.) ( $\mu$ g/L) ( <sup>a</sup> )	T <sub>max</sub> (Mouse, P.O.) (h) ( <sup>b</sup> )	T <sub>1/2</sub> (Mouse, P.O.) (h) ( <sup>c</sup> )	AUC <sub>0–inf</sub> (ng/ mL*h) ( <sup>d</sup> )	CYP1A2 [pre-inc] IC <sub>50</sub> ( $\mu$ M)	CYP2C9 [pre-inc] IC <sub>50</sub> ( $\mu$ M)	CYP2C19 [pre-inc] IC <sub>50</sub> ( $\mu$ M)	CYP2D6 [pre-inc] IC <sub>50</sub> ( $\mu$ M)	HepG2 Cytotoxicity [Glu/Gal] IC <sub>50</sub> ( $\mu$ M)	hERG IC <sub>50</sub> ( $\mu$ M)
1	 BGaz-002	5( <sup>e</sup> )	53.9	1.87	24.9	1268.03	>20 [>20]	>20 [>20]	>20 [>20]	0.19 [0.08]	38/65	173
2	 BGaz-004	5( <sup>e</sup> )	87.6	0.87	11.3	1406.8	>20 [>20]	>20 [17.78]	>15.13 [2.04]	1.97 [1.05]	>100/>100	25
3	 BGaz-005	5( <sup>e</sup> )	43.1	6	35.7	1542.4	>20 [>20]	>20 [>20]	>20 [15.79]	0.06 [0.01]	21/23	12.7

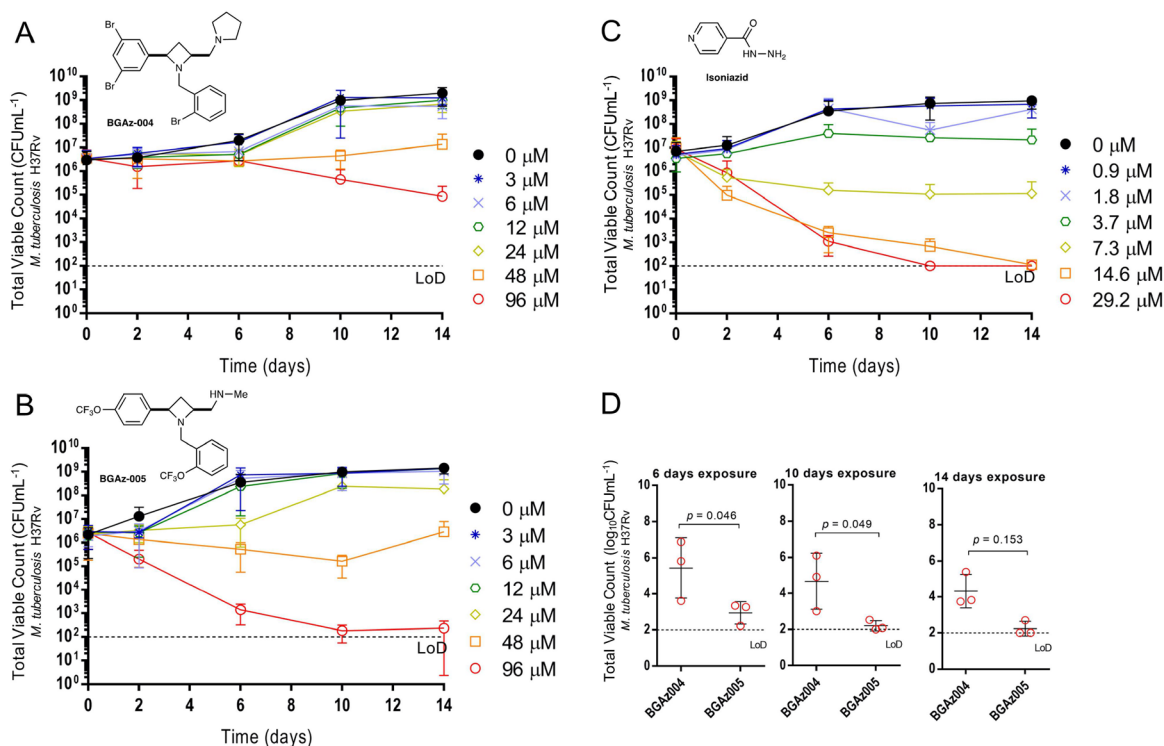
<sup>a</sup>Measures maximum peak serum concentrations of the drug. <sup>b</sup>The time of first occurrence of C<sub>max</sub>. <sup>c</sup>The terminal half-life of the drug. <sup>d</sup>The area under the plasma drug concentration–time curve to infinite time. <sup>e</sup>As a result of cassette dosing of BGaz-001–005; see the PK Data file in the Supporting Information. <sup>f</sup>Multiple daily dosing 4 × 30 mg/kg; see the PK Data file in the Supporting Information. <sup>g</sup>Multiple daily dosing 3 × 30 mg/kg; see the PK Data file in the Supporting Information.

exhibit bactericidal activity, since both MIC and MBC values overlap (Table 2).

**Physiochemical and Toxicological Properties of BGaz-002–BGaz-005.** BGaz-002–BGaz-005 were subjected to in vitro DMPK testing; BGaz-001 was excluded from further study due to its comparatively poor antimycobacterial activity. The poorer kinetic solubility BGaz-002–BGaz-004 (9 to 57  $\mu$ M) in aqueous buffered solution in comparison to the higher solubility of BGaz-005 (117  $\mu$ M) can be attributed to the presence of a secondary versus tertiary amine functionality (Table S3). Metabolic stability of the

compounds was evaluated through measuring the intrinsic clearance (CL<sub>int</sub>) by mouse liver microsomes and by liver hepatocytes. Compounds BGaz-002–BGaz-004 all exhibited a CL<sub>int</sub> of >150  $\mu$ L/min/mg in the microsomal stability assay, indicating a rapid clearance (Table S3, entries 1 to 3), with BGaz-005 giving the lowest rate of microsomal clearance (36  $\mu$ L/min/mg, Table S3, entry 4). Experiments were repeated using mouse liver hepatocytes, and all four compounds afforded CL<sub>int</sub> values of <60  $\mu$ L/min/mg, indicating good overall metabolic stability (Table S3). Caco-2 permeability assays were conducted to predict both intestinal permeability





**Figure 2.** Assessment of bactericidal activity of BGaz-004 and BGaz-005 against *M. tuberculosis* H37Rv. Average total viable counts (CFU mL<sup>-1</sup>) of *M. tuberculosis* cultures exposed to either BGaz-004 (Panel A) or BGaz-005 (Panel B) at concentrations: 0 μM (0.1% DMSO) (circle, closed), 3, 6, 12, 24, 48, and 96 μM or isoniazid (Panel C) at concentrations 0 μM (0.1% DMSO), 0.9, 1.8, 3.7, 7.3, 14.6, and 29.2 μM over a 14-day time-course. Samples were taken after 0, 2, 6, 10, and 14 days of antibiotic exposure, serially diluted, and plated by the method of Miles et al.<sup>27</sup> Statistical comparisons were performed at 6, 10, and 14 days of antibiotic exposure at 96 μM BGaz-004 and BGaz-005 using factorial ANOVA and posthoc Tukey's honestly significant difference test (Panel D). Data represent three biological repeats ± standard deviation.

and drug efflux. Compounds BGaz-002–BGaz-004 exhibited poor efflux ratios while BGaz-005 continued to perform well with an efflux ratio of less than 1.0.

The pharmacokinetic (PK) parameters of BGaz-001–BGaz-005 in a mouse model were investigated by cassette (combined) dosing at 5 mg/kg PO, 1 mg/kg IV, and IP (PK data file: Tables S1–S5). For the oral dosing, at 5 mg/kg, BGaz-001, BGaz-002, and BGaz-003 gave peak serum concentrations ( $C_{\max}$ ) of 54.7, 53.9, and 56.0 μg/L, respectively. BGaz-004 gave the highest  $C_{\max}$  whereas BGaz-005 gave the lowest, 87.6 and 43.1 μg/L, respectively (Table 3, entries 2 and 3). The plasma half-life ( $T_{1/2}$ ) of BGaz-001 was revealed to be 1.5 h, and those of BGaz-002 and BGaz-003 were 24.9 and 28.0 h, respectively. BGaz-004 has a half-life of 11.4 h, with BGaz-005 having the longest half-life of 35.7 h. BGaz-001–003 was excluded from further study due to poor PK/PD parameters. Mice were dosed multiple times with BGaz-004 and BGaz-005 (four and three times, respectively) at 30 mg/kg (PO) in order to provide evidence of compound tolerability and refinement of measured parameters. BGaz-004 and BGaz-005 gave  $C_{\max}$  values of 363.0 and 1712.5 μg/L, respectively;  $T_{1/2}$  values of 8.1 and 80.4 h were calculated, respectively (Table 3, entries 2 and 3). The total body exposure from multiple dosing at 30 mg/kg (PO) of BGaz-005 (82247.7 ng/mL·h) was significantly greater than BGaz-004 (5420.99 ng/mL·h), indicating a superior overall pharmacokinetic profile for BGaz-005 (Table 3, entries 2 and 3). BGaz-002, BGaz-004, and BGaz-005 were tested for cytochrome P450 (CYP450) metabolic activity by measuring the inhibition of each of specific enzymes in human liver

microsomes. All three compounds exhibited no discernible inhibition of CYP1A2, an enzyme known to metabolize aromatic/heterocyclic amine-containing drugs (Table 3). The CYP2C9 enzyme is a relatively abundant CYP450 in the liver that dominates CYP450-mediated drug oxidation. In this regard, only minimal CYP2C9 inhibition when BGaz-004 was preincubated for 30 min prior to the addition of NADPH to initiate catalysis was observed. Known to metabolize a wide range of drug molecules, CYP2C19 is an essential member of the CYP450 superfamily as it contributes ~16% of total hepatic content in humans. BGaz-002 and BGaz-005 displayed only negligible inhibition of this enzyme, BGaz-004 displayed strong inhibitory activity when preincubated for 30 min prior to initiation of catalysis (Table 3). CYP2D6 is widely implicated in the metabolism of drugs that contain amine functional groups, such as monoamine oxidase inhibitors and serotonin reuptake inhibitors. CYP2D6 is responsible for the second highest number of drugs metabolized by the CYP450s, as demonstrated by the significant inhibition of this enzyme by BGaz-002, BGaz-004, and BGaz-005. All three compounds were evaluated for mitochondrial dysfunction by measuring IC<sub>50</sub> values against HepG2 cells cultured in media containing either glucose or galactose, which serves to direct cellular metabolic activity toward glycolysis or oxidative phosphorylation, respectively. While BGaz-004 exhibited a negligible effect, both BGaz-002 and BGaz-005 demonstrated cytotoxicity with IC<sub>50</sub> values of 38 and 21 μM, respectively (Table 3). To enhance cellular susceptibility to mitochondrial toxicants, assays were repeated in the presence of galactose, which resulted in Glu/Gal ratios

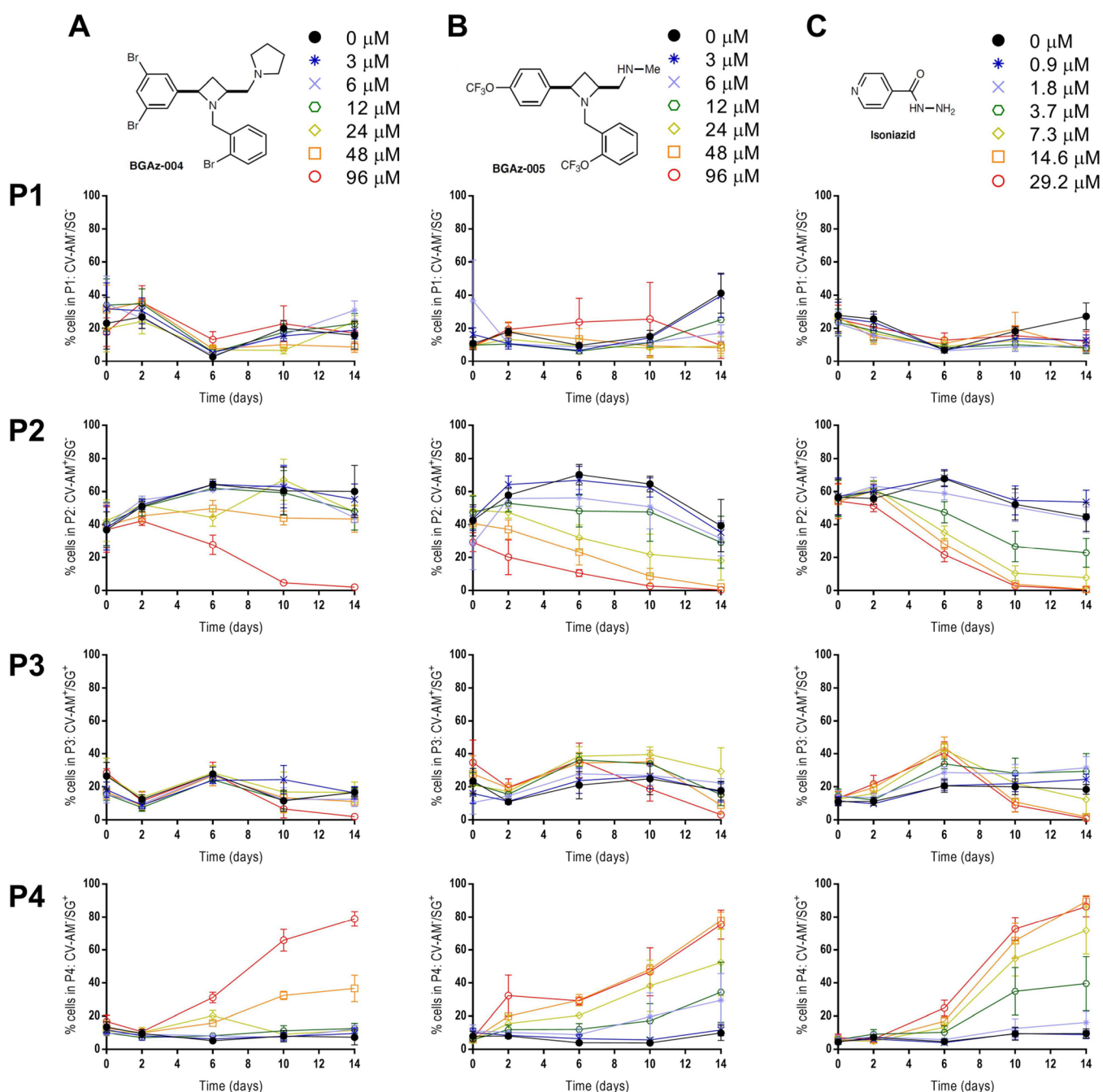


**Figure 3.** Assessment of bactericidal activity of BGaz-004 and BGaz-005 against *M. tuberculosis* H37Rv. Quantitation of Calcein-Violet-AM (CV-AM) and Sytox-green (SG) fluorescence of *M. tuberculosis* H37Rv, using flow cytometry, after exposure to BGaz-004 (column A) and BGaz-005 (column B) at concentrations: 0  $\mu$ M (0.1% DMSO), 3, 6, 12, 24, 48, and 96  $\mu$ M or (column C) isoniazid at concentrations 0  $\mu$ M (0.1% DMSO), 0.9, 1.8, 3.7, 7.3, 14.6, and 29.2  $\mu$ M over a 14-day time-course. The percentages of the population that are unstained or stained with each dye (or both dyes) are represented in four gates (rows P1–P4). Row P1: unstained population (CV-AM<sup>-</sup>/SG<sup>-</sup>); row P2: CV-stained population (CV-AM<sup>+</sup>/SG<sup>-</sup>); row P3: dual-stained population (CV-AM<sup>+</sup>/SG<sup>+</sup>); and row P4: SG-stained population (CV-AM<sup>-</sup>/SG<sup>+</sup>). Data represent three biological repeats  $\pm$  standard deviation. Statistical comparisons were made using factorial ANOVA and *posthoc* Tukey's honestly significant difference test.

of  $<1$ , confirming no mitochondrial toxicity. Compounds BGaz-002, BGaz-004, and BGaz-005 were assayed for hERG inhibition using *IonWorks* patch clamp electrophysiology. An eight-point concentration–response curve was generated from a three-fold serial dilution of a top compound concentration of 167  $\mu$ M. Compound BGaz-002 was the best performing compound, displaying a hERG liability IC<sub>50</sub> of 173  $\mu$ M, (i.e., inhibition of less than 50% at the top 167  $\mu$ M test

concentration). In comparison, compounds BGaz-004 and BGaz-005 performed significantly worse with hERG liability IC<sub>50</sub> of 25 and 12.7  $\mu$ M, respectively. Overall, the BGaz compounds investigated in this preliminary study display an encouraging toxicological and PK/PD profile to enable further exploration and development toward clinics.

**BGaz Compounds Kill *M. tuberculosis* with Bactericidal Activity.** The bactericidal activity of BGaz-004 and

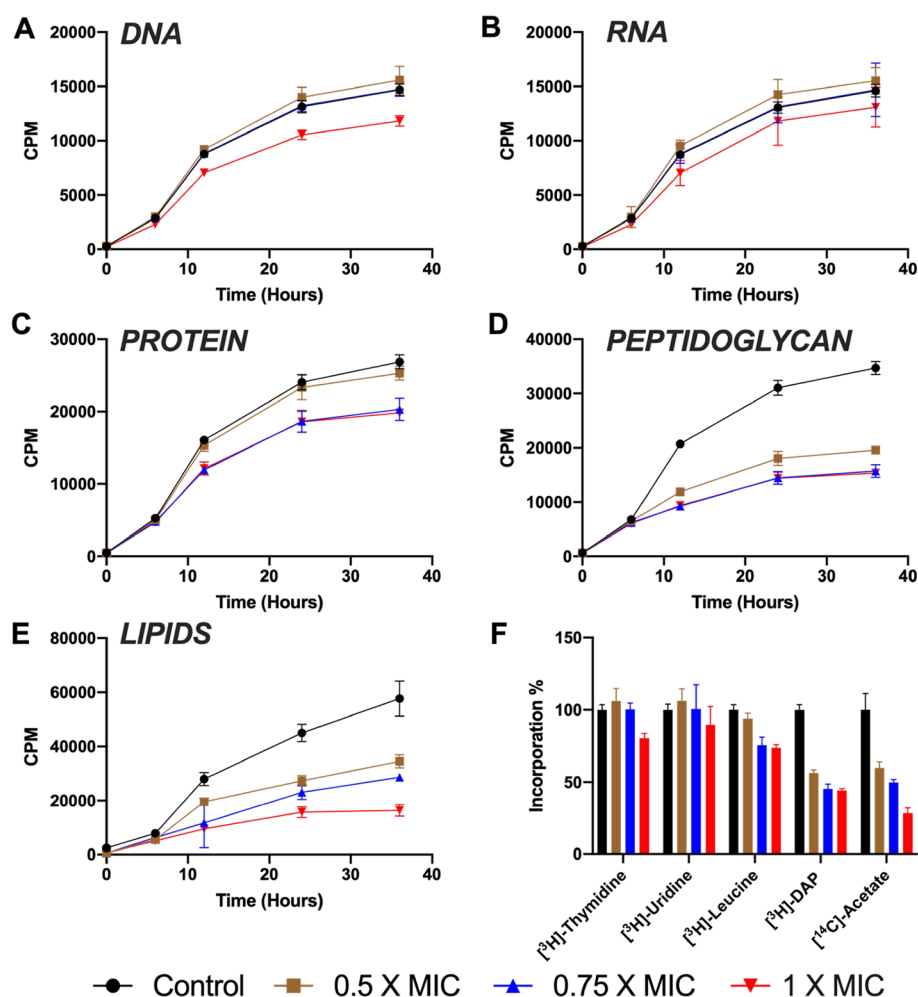


**Figure 4.** Effect of BGAz-005 on the incorporation of radiolabeled precursors into the major cellular macromolecules of *M. smegmatis*. The incorporation of (A) [*methyl*- $^3\text{H}$ ]thymidine (for DNA), (B) [*S*,6- $^3\text{H}$ ]uridine (for RNA), (C) L-[4,5- $^3\text{H}$ ]leucine (for protein), (D) [ $^3\text{H}$ ]meso-diaminopimelic acid (for peptidoglycan), and (E) [ $^{14}\text{C}$ ]acetic acid (for lipids) was measured over a period of 36 h. The percentage of incorporation measured at 36 h is represented in panel F. Each plot and error bars represent the average of three independent experiments.

BGAz-005 against *M. tuberculosis* H37Rv was further assessed by exposing the bacilli to a range of concentrations of BGAz-004 and BGAz-005 over a time-course of 14 days and total viable counts (CFU mL<sup>-1</sup>) enumerated on solid medium. Both BGAz-004 and BGAz-005 were active against *M. tuberculosis* H37Rv (Figure 2, panels A and B), with BGAz-005 demonstrating statistically significantly greater early bactericidal and concentration-dependent activity than BGAz-004 at day 6 ( $P = 0.046$ ) and day 10 ( $P = 0.049$ ) (Figure 2D). Exposure of *M. tuberculosis* H37Rv to BGAz-005 resulted in a greater bactericidal effect with more pronounced activity earlier in the time-course, with a reduction of  $3.28 \pm 1.00 \log_{10}$  CFU mL<sup>-1</sup> after 6 days of exposure and reduction of  $3.99 \pm 0.60 \log_{10}$  CFU mL<sup>-1</sup> after 14 days' exposure, at a concentration of  $96 \mu\text{M}$  (Figure 2B). Equivalent activity was not observed by BGAz-004 early in the time-course and showed delayed activity at all concentrations, only achieving a decrease in  $0.79 \pm 2.20 \log_{10}$  CFU mL<sup>-1</sup> by day six and  $1.90 \pm 1.28 \log_{10}$  CFU mL<sup>-1</sup> reduction after 14 days at  $96 \mu\text{M}$  (Figure 2A). The profile for BGAz-004 is commensurate with antibiotics that exhibit bacteriostatic activity at lower concentrations. Isoniazid demonstrated a higher rate of bactericidal activity compared to both BGAz-004 and BGAz-005 by achieving a reduction of  $>4.52 \pm 0.60 \log_{10}$  CFU mL<sup>-1</sup>

to a limit of detection ( $100 \text{ CFU mL}^{-1}$ ), by day 10, at a lower concentration of  $29 \mu\text{M}$  (Figure 2C).

In addition to the enumeration of viable bacilli on agar, the activity of BGAz-004 and BGAz-005 was determined using flow cytometry. This approach allows for a direct assessment of whether BGAz compounds are able to kill *M. tuberculosis* in a dose-dependent manner and whether the killing profile was similar between these compounds and to that observed for isoniazid, which would provide insights about their mode of action.<sup>28</sup> Culture samples were taken at each time-point and dual-stained using Calcein Violet with an acetoxymethyl ester group (CV-AM) that is a correlate of metabolic activity, and Sytox Green (SG) that enables measurement of cell-wall permeability (a proxy for cell death). Single bacilli were identified by forward scattered light area and height using flow cytometry analyses. Gated single cells were further differentiated based on the presence and absence of CV-AM and SG staining using a quadrant gating approach. The percentages of the population that are unstained or stained with each dye (or both dyes) are represented in four gates P1–P4 (P1: CV-AM<sup>-</sup>/SG<sup>-</sup>, P2: CV-AM<sup>+</sup>/SG<sup>-</sup>, P3: CV-AM<sup>+</sup>/SG<sup>+</sup>, P4: CV-AM<sup>-</sup>/SG<sup>+</sup>) (Figure 3). The CV-AM staining profiles (metabolic activity) for these compounds were reflective of the total viable counts (Figure); the decrease in CV-AM

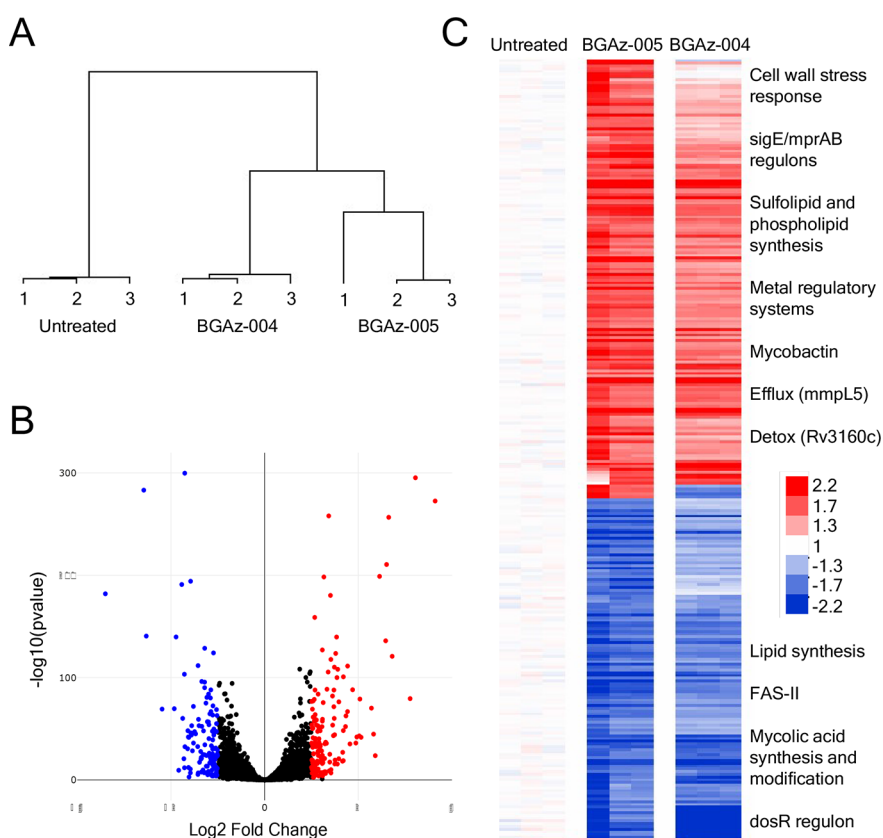


**Figure 5.** Transcriptional response to **BGAz-005** exposure demonstrating inhibition of mycobacterial cell envelope biosynthesis. (A) Cluster diagram of all genes showing similarity of biological replicates and separation of drug-treated from carrier control samples. (B) Volcano plot of *M. bovis* BCG response to **BGAz-005**, highlighting genes significantly differentially expressed. (C) Heatmap of 286 gene **BGAz-005** signature relative to carrier control. Conditions as columns, genes as rows; red coloring highlighting induced genes and blue representing repressed genes. The **BGAz-004** signature is clustered alongside, indicating a similar mode of drug action.

staining over the time-course at 96  $\mu\text{M}$  for **BGAz-005** was statistically significant after day 6 ( $P = 0.043$ ), day 10 ( $P = 0.08$ ), and day 14 ( $P = 0.011$ ) compared to the decrease in the CV-AM staining for **BGAz-004**, at the same concentration (Figure 3A,B; P2). A similar difference in activity was observed at 48  $\mu\text{M}$ , ( $P = 0.067$ , 0.065, 0.066 for days 6, 10, and 14, respectively). The SG-staining profiles showed that both compounds possessed equivalent killing activity at high concentrations of 96  $\mu\text{M}$  (Figure 3A,B; P4); however, **BGAz-005** shows higher levels of kill at days 6 and 14 with a lower concentration of 48  $\mu\text{M}$  ( $P = 0.027$  and 0.068, respectively). Both **BGAz-004** and **BGAz-005** show similar staining profiles to isoniazid (Figure 3C), which targets the mycobacterial cell wall.<sup>28</sup>

**BGAz-004 and BGAz-005 Inhibit the Incorporation of Mycobacterial Cell Wall Precursors and Display No Detectable Resistance.** Whole genome sequencing (WGS) of laboratory-generated mutants that are resistant to TB drugs is a widely used approach to determine the mode of action of novel antibacterial compounds.<sup>29–31</sup> Multiple attempts (>5 biological repeats) to generate drug-resistant mutants of **BGAz-002–BGAz-005** in *M. smegmatis* and *M. bovis* BCG (including a strain of BCG devoid of *recG* which has a higher mutational frequency)<sup>32</sup> were unsuccessful, implying an undetectably low frequency of resistance for these compounds (Supporting Information). This advantageous property is a double-edged sword. The discovery of the BGAz series as novel antitubercular compounds with low frequencies of

resistance is attractive in terms of drug development, especially in the context of MDR-TB; however, the inability to generate resistant mutants against the most active compounds suggests that this series of compounds may elicit pleiotropic activity or have nonspecific modes of action, or nonprotein target(s). Therefore, in order to investigate the mode of action of **BGAz-005**, the most active of the compounds tested against mycobacteria, biosynthetic inhibition of five major macromolecular pathways was evaluated by measuring the incorporation of selected radiolabeled precursors during microbial cell culture. The addition of **BGAz-005** up to a concentration of  $0.75 \times \text{MIC}$  had almost no effect on the incorporation of [ $^3\text{H}$ ]-thymidine, [ $^3\text{H}$ ]-uridine, and [ $^3\text{H}$ ]-leucine with only a moderate 20% reduction of incorporation at  $1 \times \text{MIC}$ , suggesting that **BGAz-005** does not directly inhibit DNA, RNA, or protein biosynthesis (Figure 4). In contrast, **BGAz-005** decreased the incorporation of both [ $^3\text{H}$ ]-DAP and [ $^{14}\text{C}$ ]-acetic acid from 6 h postlabeling and, at  $0.5\times$  and  $1 \times \text{MIC}$ , caused a titratable decrease in [ $^{14}\text{C}$ ]-acetic acid incorporation, exerting a  $\sim 50$  and  $\sim 75\%$  loss of lipid biosynthesis, respectively (Figure 4). These data suggest that the **BGAz-005** acts by inhibiting aspects of mycobacterial cell envelope biosynthesis.

**BGAz-005 Dysregulates the Expression of Cell Envelope Biosynthetic Genes.** To explore the mode of action of **BGAz-005** using an unsupervised approach, the *M. bovis* BCG transcriptional response to drug exposure was profiled by RNaseq A signature consisting of 160 induced and



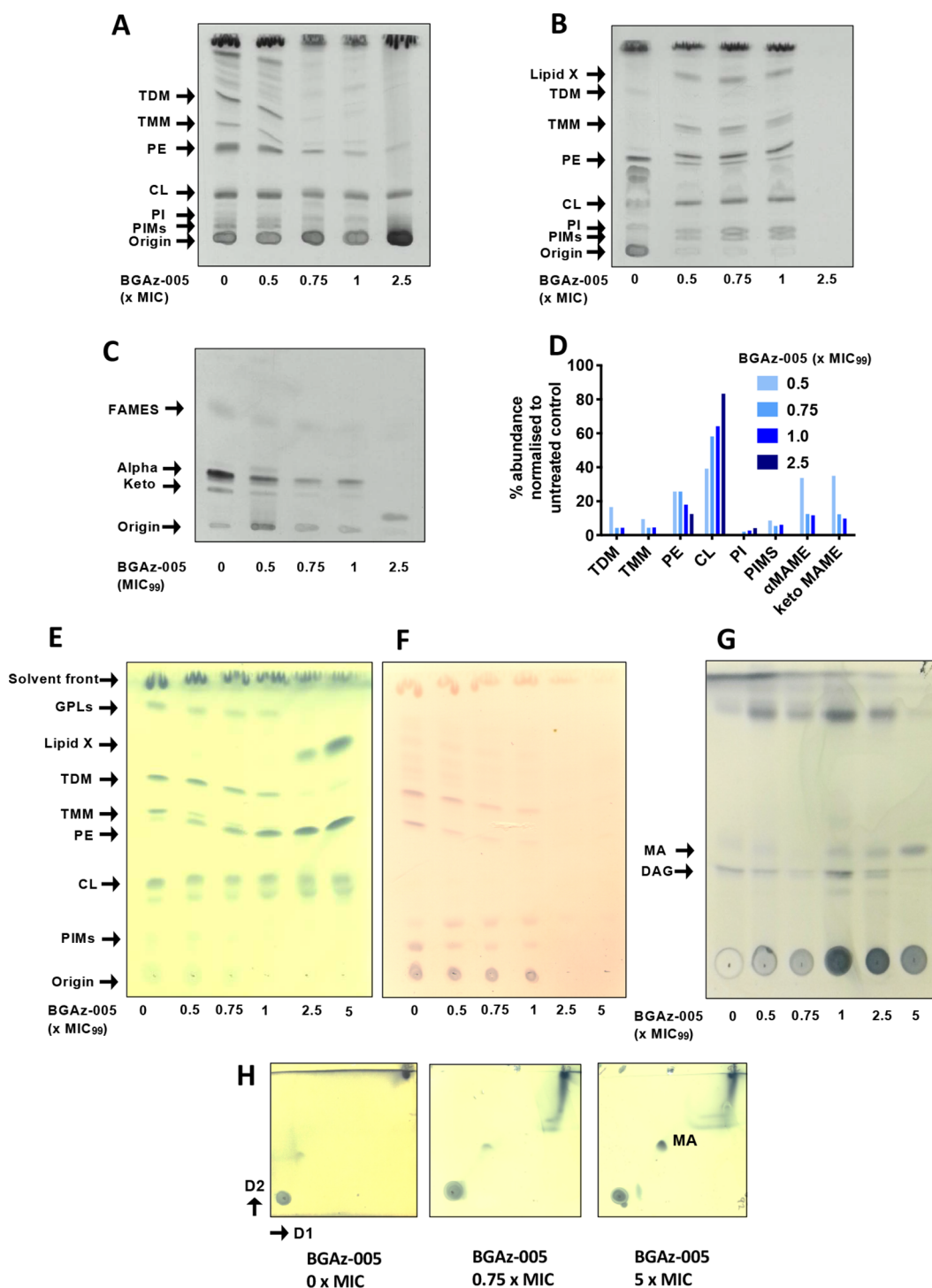


**Figure 6.** BCG cell envelope lipid analysis upon exposure to BGaz-005. BCG were cultured in 7H9 broth and exposed to increasing concentrations of BGaz-005. Lipids were selectively labeled with [<sup>14</sup>C]-acetic acid for 12 h, and cell envelope lipids were selectively removed by solvent extraction, separated by TLC (chloroform/methanol/water, 80:20:2, v/v/v), and visualized by autoradiography. (A) Equal volumes of lipids loaded adjusted for BCG growth; (B) equal counts of lipids (25,000 cpm) loaded; (C) mycolic acid methyl ester (MAME) analysis of cell-wall bound mycolates released by 5% TBAH and separated by TLC (petroleum ether/acetone, 95:5, v/v); (D) quantification of BCG lipids from panels A–C by densitometry. *M. smegmatis* cell envelope lipid analysis upon exposure to BGaz-005. (E) *M. smegmatis* were cultured in 7H9 broth, exposed to increasing concentrations of BGaz-005 for 6 h and the cell envelope lipids selectively removed by solvent extraction. Equal volumes of lipid adjusted by bacterial growth were separated by TLC (chloroform/methanol/water, 80:20:2, v/v/v) and stained with MPA or (F) alpha-naphthol. (G) Equal volumes of lipid adjusted by bacterial growth were separated by TLC (hexane/diethyl ether/acetic acid), 70:30:1, v/v/v and stained with MPA. (H) Equal volumes of lipid adjusted by bacterial growth were separated by 2D-TLC (direction 1 chloroform/methanol 96:4, v/v, direction 2 toluene/acetone 80:20, v/v) and stained with MPA.

126 repressed genes was identified after 8 h' exposure to 1 × MIC BGaz-005. The response was comprised of three

principal features, namely, inhibition of cell wall biosynthesis, dysregulation of metal homeostasis, and disruption of the

respiratory chain (Figure 5). The inhibition of cell wall synthesis was evidenced by induction of key regulators of cell wall stress *sigE* and *mprAB*, alongside significant upregulation of their regulons (hypergeometric *p* value of *sigE* regulon enrichment  $2.47 \times 10^{-17}$ ; *mprAB* hgp  $5.29 \times 10^{-11}$ ).<sup>34</sup> In contrast to isoniazid and ethambutol where *FasII* genes are induced by drug exposure, *FasII* genes (*hadA*, *fabG1*, *inhA*, *acpM*) alongside mycolic acid synthesis and modification genes (*mmaA2*, *mmaA3*, *fbpA*, *fbpB*, *fbpD*, and *desA2*) were repressed by BGaz-005 treatment, indicating a different mechanism of BGaz-005 drug action to cell wall inhibitors currently in use. The functional category (I.H) lipid biosynthesis was significantly repressed by BGaz-005 (hgp  $6.52 \times 10^{-5}$ ), and mycolyl-arabinogalactan-peptidoglycan complex biosynthesis was the top pathway dysregulated by BGaz-005 (pathway perturbation score of 3.4).<sup>35,36</sup> Genes involved in the synthesis of alternative cell wall factors, sulfolipids (*mmpL8*, *papA1*, and *pks2*) and the oleic acid stearoyl-CoA desaturases that produce phospholipids (*desA3\_1*, *desA3\_2*, and *BCG\_3260c/Rv3230c*), were induced.<sup>37</sup> A series of metal-responsive regulatory systems were upregulated by BGaz-005 (*cmtR*, *zur*, *ideR*, and *tcyYX*) as well as genes encoding the lipid-bound siderophore mycobactin (*mbtB*, *mbtC*, and *mbtD*), representing disruption of metal control systems, likely impacted by loss of cell-wall structure. Induction of redox-inducible *clgR* in combination with repression of the *dosR* regulon (hgp  $6.40 \times 10^{-9}$ ) reflected the impact of BGaz-005 on the respiratory chain.<sup>38</sup> However, unlike many drugs that affect respiration, no differential expression of energy metabolism systems (*nuoA-N*, *qcrA-C*, *ctaC-E*, *cydA-D*, and *narG-J*) was observed.<sup>39,40</sup> Systems implicated in the efflux (*mmpL5*, *mmpS5*, *BCG\_0727/Rv0678*, and *BCG\_0728c/Rv0679c*) or detoxification (*BCG\_3184c/Rv3160c*, *BCG\_3185c/Rv3161c*, and *BCG\_3186c/Rv3162c*) of antimicrobial drugs were also induced by BGaz-005.<sup>41</sup> Significantly, the efflux pump *efpA*, highly induced by cell wall targeting drugs isoniazid, ethambutol, and benzothiazinone, was not induced by BGaz-005 exposure.

Mapping the drug-responsive gene clusters identified by Boshoff and co-workers revealed significant enrichment of GC-27 and GC-82 representing cell wall inhibition,<sup>42</sup> alongside GC-39 (*dosR* regulon) and GC-108 (iron scavenging). The most similar drug signatures were the phenothiazines, chlorpromazine, and thioridazine (hgp  $2.83 \times 10^{-14}$ ), disrupting the cell wall and electron transfer chain,<sup>43</sup> alongside analogues of ethambutol (hgp  $4.98 \times 10^{-13}$ )<sup>44</sup> and benzothiazinone (hgp  $8.00 \times 10^{-8}$ ) targeting arabinose biosynthesis in the mycobacterial cell wall.<sup>45</sup> Thus, BGaz-004 and BGaz-005 elicit a transcriptomic response representing major abrogation of normal cell envelope function.

**BGAz-004 and BGaz-005 Significantly Alter Mycobacterial Cell Envelope Composition.** The results of transcriptomic profiling and whole cell phenotyping support the hypothesis that BGaz-004 and BGaz-005 inhibit aspects of cell envelope biosynthesis. To further investigate the mechanism by which mycobacterial cell envelope lipid composition is affected, actively growing cultures of BCG were exposed to increasing concentrations of BGaz-005 followed by metabolic labeling using [<sup>14</sup>C]-acetic acid. Autoradiographs of cell envelope lipids separated by thin layer chromatography (TLC) revealed that treatment of BCG with BGaz-005 at  $0.5 \times \text{MIC}$  caused a significant reduction in trehalose monomycolate (TMM) and trehalose dimycolate

(TDM) and a complete loss of TMM and TDM at concentrations beyond the MIC (Figure 6A). The formation of cytoplasmic membrane phospholipids (PIMs and CL) remains unaffected (Figure 6A). The analysis of lipids loaded and separated by TLCs that had been normalized for total lipids extracted revealed an altered lipid profile, highlighting the accumulation of an unidentified lipid species that resolves to a relatively high *R<sub>f</sub>* (Lipid species X, Figure 6B). The analysis of mycolic acid methyl esters (MAMES) reveals that both alpha and keto mycolates bound to the cell wall arabinogalactan (AG) are gradually depleted, as BCG is exposed to increasing concentrations of BGaz-005 during active cell culture (Figure 6C). Quantification of the relative abundance of each lipid species highlights the significant depletion of mycolates (either conjugated to trehalose in the form of TMM/TDM or AG) when BGaz-005 is used at a half MIC, while other lipids including PI and PIMS remain largely unaffected (Figure 6D). BGaz-004 affects mycobacterial cell envelope lipid biosynthesis in an almost identical manner (Figure S3). The immediate and specific arrest in the biosynthesis of TMM and TDM, and as a result, loss of esterified mycolates to AG, strongly supports the hypothesis that BGaz-004 and BGaz-005 inhibit mycobacteria by targeting mycolate biosynthesis.

To investigate the effect of BGaz-005 on mycobacterial cell envelope composition and to identify the composition of Lipid-X, actively growing cultures of *M. smegmatis* were exposed to a range of BGaz-005 concentrations, which resulted in a titratable-dependent reduction in the formation of TMM and TDM as observed by staining with MPA and  $\alpha$ -naphthol (Figure 6E/F), consistent with [<sup>14</sup>C]-labeling experiments performed when BGaz-005 was exposed to BCG (Figure 6). *M. smegmatis* exposed to the highest concentration of BGaz-005 resulted in a significant increase in the relative abundance of free mycolic acid (MA) within the cell envelope (Figure 6G); BGaz-004 affects mycobacterial cell envelope lipid biosynthesis in an almost identical manner (Figure S4). The gradual reduction of TMM and TDM abundance in *M. smegmatis* and *M. bovis* BCG is a distinct observable phenotype that occurs upon exposure to BGaz-005 (Figures 6 and S3 and S4). The separation of solvent-extractable lipids by two-dimensional TLC provides further confirmatory evidence that the increasing abundance of Lipid-X can be directly attributed to free MA.<sup>46</sup> This large increase in free mycolic acid, paralleled with the loss of TMM, TDM, and arabinogalactan-linked mycolates, illustrates that BGaz-005 (and BGaz-004) compounds kill mycobacteria by arresting the final stages of mycolate biosynthesis.

**BGAz-004 and BGaz-005 Target Late-Stage Mycolic Acid Biosynthesis Enzymes.** The inhibition of mycolate incorporation into the mycobacterial cell wall, supported by transcriptomic profiling, suggests that BGaz-004 and BGaz-005 act by targeting late-stage mycolate biosynthesis (Figures 5 and 6). The accumulation of free mycolic acid upon exposure to BGaz-004 and BGaz-005 at the highest concentrations suggests that mycolates are being formed but not deposited into the cell wall (Figures 6 and S4). *Pks13*, *MmpL3*, and the *Ag85* complex (*FbpA*, *FbpB*, and *FbpC*) represent a selection of putative enzyme targets of mycolate biosynthesis that could be inhibited by BGaz-004 and BGaz-005. *Pks13* catalyzes the last condensation reaction in mycolate biosynthesis, condensing two fatty acids to form mycolic acids.<sup>47</sup> It also plays a role in TMM formation through acylation of trehalose.<sup>48</sup> Although

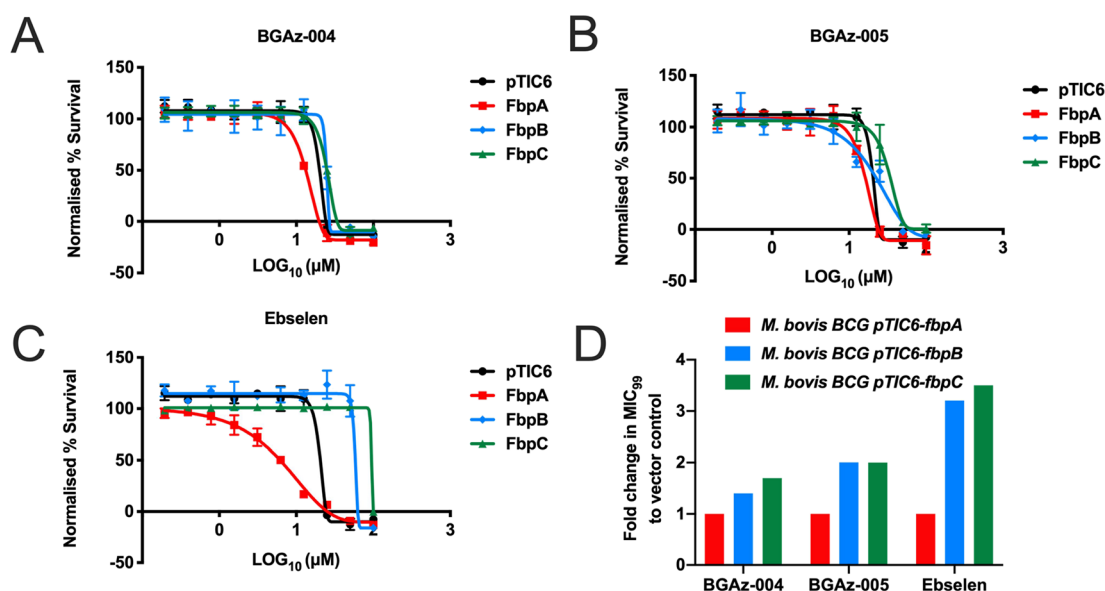


**Figure 7.** Assessing the MIC shift of BGaz-004 and BGaz-005 against the AG85 complex. MIC values of BGaz-004, BGaz-005, and Ebselen were determined against BCG harboring overexpression vectors and compared to empty vector controls (pTIC6) in order to identify a shift in MIC against fbpA (A), fbpB (B), and fbpC (C). Fold change in MIC shift (D). The MIC<sub>99</sub> was calculated using an end point resazurin assay and the Gompertz equation for MIC determination (GraphPad Prism). Data are of triplicate repeats.

essential in mycobacteria, *Corynebacterium glutamicum* can survive without mycolates,<sup>47</sup> and so a Pks13 deletion mutant of *C. glutamicum* was utilized in this study (Supporting Information). BGaz-005 inhibits corynemycolic acid biosynthesis in *C. glutamicum* in a manner similar to mycobacteria (Figure S6). BGaz-002–BGaz-005 retained similar levels of activity in *C. glutamicum*Δpks13 as in the wild-type strain, implying that Pks13 is not the target (Table S2). MmpL3 is the essential membrane transporter responsible for translocating TMM across the cytoplasmic membrane.<sup>46,49</sup> Treatment of *M. bovis* BCG harboring an MmpL3 overexpression vector (pMV261A-mmpL3)<sup>50</sup> with BGaz-002–BGaz-005 resulted in no shift in the MIC<sub>99</sub> compared to the empty vector (pMV261A) control (Table S2). This negates MmpL3 as a potential target of the active BGaz compounds in this study, as overexpression of mmpL3 should result in an increase in MIC as a result of increased copy number and target abundance. The Ag85 complex consists of three essential enzymes with mycolyltransferase activity, responsible for the formation of TMM, TDM, and the covalent attachment of mycolic acids to arabinogalactan.<sup>51</sup> BCG harboring the plasmids pTIC6-fbpA, pTIC6-fbpB, and pTIC6-fbpC overexpressing Ag85A, Ag85B and Ag85C, respectively, were treated with BGaz-004 and BGaz-005. A statistically significant increase in MIC was seen with FbpB and FbpC, but not FbpA (Figure 7). A two-fold increase in MIC was seen for both BGaz-004 and BGaz-005 upon overexpression of FbpB and FbpC, compared to the three-fold increase seen with known covalent inhibitor Ebselen.<sup>52</sup> No shift in MIC was seen for FbpA upon Ebselen treatment. Furthermore, *M. smegmatis* cultured in the presence of Ebselen also resulted in a significant increase of free mycolic acid (MA) within the cell envelope and a concomitant loss of TMM and TDM (Figure S5), mirroring the lipid profiles induced by BGaz-004 and BGaz-005. Collectively, these findings point toward the antigen 85 enzymes as a possible target of the active BGaz compounds of this study.

## DISCUSSION AND CONCLUSIONS

The emergence of multidrug-resistant TB means that new drugs to treat this disease are desperately required. Any new therapy should meet a number of parameters: it should be effective against MDR-TB; it should be rapidly bactericidal; it should show a novel mechanism of action; and it should possess ADME properties suitable for once-a-day oral dosing and coadministration with the current TB therapies and anti-HIV agents.<sup>53</sup> BGaz-002–BGaz-005 display potent inhibitory activity against different mycobacterial species (including virulent and avirulent *M. tuberculosis* reference strains), as well as drug-sensitive and drug-resistant (resistant to isoniazid, rifampicin, pyrazinamide, and ethambutol) clinical isolates of *M. tuberculosis*. It is promising that BGaz-002–BGaz-005 retain similar levels of activity between drug-sensitive and drug-resistant clinical isolates of *Mtb*; not only do these compounds target MDR-TB, but this also suggests that there is no cross-resistance with the current frontline drugs, indicative of a distinct mode of action. In addition to targeting an MDR strain of *Mtb*, the active BGaz compounds tested display no detectable resistance against mycobacteria in the laboratory, suggesting that the development of clinical resistance to this class of compounds will be slow to occur. Similarly, teixobactin is a cyclic undecapeptide antibiotic that elicits bactericidal activity toward clinically relevant Gram-positive pathogens, also displaying an undetectable frequency of resistance. Teixobactin has a unique mode of action; by binding simultaneously to the cell-wall biosynthetic precursors lipid II and Lipid III, this antibiotic inhibits the biosynthesis of peptidoglycan and cell-wall teichoic acids, respectively.<sup>54</sup>

For each of BGaz-002–BGaz-005, the MBC is within four-fold of the MIC<sub>99</sub>, demonstrating their bactericidal nature in BCG. Further assessment in *M. tuberculosis* by time-kill viable counts and flow cytometry confirmed the bactericidal activity of BGaz-004 and BGaz-005, with BGaz-005 being significantly bactericidal after 6 days. The significantly earlier bactericidal activity of BGaz-005 compared to BGaz-004



could be attributed to the increased kinetic solubility of **BGAz-005**, or it could suggest that **BGAz-005** has additional targets. While neither **BGAz-004** nor **BGAz-005** displayed bactericidal activity as rapidly as the current frontline drug isoniazid,<sup>55</sup> the slower killing induced by the BGAz compounds tested may prove advantageous in preventing bacterial regrowth.<sup>56</sup> Previous studies have shown that the rapid, early bactericidal activity of isoniazid results in bacterial regrowth, compared to no regrowth seen with the slower-acting bactericidal drugs rifampicin and pyrazinamide.<sup>56</sup> The longer-acting bactericidal activity of the BGAz compounds tested, combined with the absence of any detectable generation of resistance, suggests that they may be superior to isoniazid, as the potential for tolerance and resistance is very low.

The comprehensive mode of action studies supports the hypothesis that the BGAz compounds target mycobacterial cell wall biosynthesis. Radiolabeled precursor incorporation studies demonstrate that **BGAz-005** specifically arrests peptidoglycan and lipid biosynthesis, and transcriptome signatures of **BGAz-004**- and **BGAz-005**-treated *M. bovis* BCG reveal significant alterations in cell wall biosynthetic genes. The mycobacterial cell wall is a well-validated and commonly occurring target among antitubercular drugs, including frontline drugs isoniazid<sup>57</sup> and ethambutol,<sup>58</sup> as well as ethionamide,<sup>57</sup> SQ109,<sup>59</sup> and D-cycloserine.<sup>60</sup> While the BGAz compounds tested in this study also inhibit cell wall biosynthesis, they do so without displaying target redundancy against current front-line drugs, such as isoniazid. Transcriptomic analysis revealed marked differences between the **BGAz-004**, **BGAz-005**, isoniazid, and ethambutol, specifically the downregulation of mycolic acid synthesis genes of the FasII system and mycolic acid synthesis and modification genes, and the lack of induction of the *efpA* efflux pump. Compared to other genome-wide transcriptional studies of antitubercular drugs,<sup>61</sup> the observed differences induced by BGAz compounds suggest that they possess a unique mode of action compared to current chemotherapeutic agents.

To further probe the mechanisms by which the BGAz compounds perturb the mycobacterial cell envelope, the lipid profiles of mycobacteria exposed to increasing concentrations of **BGAz-005** were examined. A specific and rapid depletion in TMM and TDM was seen upon BGAz treatment of both *M. smegmatis* and *M. bovis* BCG, while other lipids such as cardiolipin and PIMs remained constant. The effects are more pronounced in BCG due to its increased sensitivity of radiolabeling, but in both instances, there is an almost complete arrest in TMM and TDM production by  $1 \times \text{MIC}$  of **BGAz-005**. Analysis of the cell-wall bound mycolates revealed a concurrent depletion in MAMEs. The specific loss in mycolates, both noncovalently (TMM and TDM) and covalently (MAMEs) associated, indicates that the BGAz compounds tested target mycolic acid biosynthesis. Mycolates are an essential component of the mycobacterial cell envelope and are targeted by the current drugs isoniazid and ethionamide.<sup>62</sup> The BGAz compounds tested target the same biosynthetic pathway as isoniazid corroborates with the flow cytometry analysis, where the staining profiles of **BGAz-004** and **BGAz-005** were like those of isoniazid, suggesting a similar target. Further cell envelope analysis revealed a pronounced increase in free mycolic acid correlating with increasing concentration of **BGAz-005**. Typically, the relative abundance of free MA in the cell envelope of planktonically cultured mycobacteria is extremely low. However, previous

studies have demonstrated that free MA levels increase significantly when mycobacteria are cultured as pellicle biofilms<sup>63</sup> or as nonreplicating populations induced by gradual nutrient starvation.<sup>64</sup> This simultaneous depletion of mycolates conjugated to trehalose and AG, alongside an accumulation of free mycolic acid, implies that the mycolates are being synthesized (demonstrated by the accumulation of free mycolate) but are not incorporated into the cell wall (demonstrated by the loss of TMM, TDM, and MAMEs). Thus, unlike isoniazid, the BGAz compounds tested target late-stage mycolic acid biosynthesis and have a mode of action distinct from that of isoniazid and Ethionamide, which target the early stages of mycolate production.<sup>57</sup> There are several enzyme candidates involved in the latter stages of mycolic acid biosynthesis and incorporation into the cell envelope. Specifically, these encode the polyketide synthase (Pks13) responsible for the last condensation reaction in mycolate biosynthesis,<sup>47</sup> the essential membrane transporter responsible for translocating TMM across the cytoplasmic membrane (MmpL3),<sup>46,49</sup> and the mycolyltransferase responsible for the formation of TMM, TDM, and the covalent attachment of mycolic acids to arabinogalactan by the antigen 85 complex enzymes (FbpA, FbpB, and FbpC).<sup>51</sup> Target engagement overexpression studies ruled out MmpL3 as a BGAz target, while experiments conducted in *C. glutamicum* demonstrate that Pks13 is equally not inhibited by these compounds. Guided by evidence obtained from transcriptomic profiling and cell envelope lipid analysis, further target engagement overexpression studies revealed that FbpB and FbpC afforded moderate protection to BCG exposed to **BGAz-004** or **BGAz-005**. Previous studies have identified FbpA, FbpB, and FbpC as druggable targets for the development of new antitubercular agents;<sup>52,65–67</sup> however, many of these agents display unfavorable toxicological and PK/PD profiles. In this regard, the BGAz compound series demonstrates an encouraging overall toxicological profile with good absorption, low mitochondrial toxicity, and rapid clearance from hepatocytes. To reduce the potential of compound-related risk factors, a selection of mechanistic screening assays was utilized to identify hazardous and undesirable chemistry in this study. A critical example of such compound liabilities is the blocking of the hERG potassium channel. The hERG channel is a voltage-gated potassium channel that is expressed in a variety of human tissues such as the brain, thymus, adrenal gland, retina, and cardiac tissue. Any significant blocking of hERG channels by potential drug candidates could have serious off-target effects due to the dysregulation of action potential repolarisation. Furthermore, **BGAz-005** displays a remarkable pharmacokinetic profile in mice, with a blood plasma half-life exceeding 3 days that exceeds the  $C_{\text{max}}$  required to reach a therapeutic dose for MDR-TB. Overall, the results presented here demonstrate that the BGAz compound series represents promising novel antitubercular agents for further development. In addition to this publication, we have patented these molecules.<sup>85</sup> The present invention relates to azetidine compounds and their uses. In particular, the invention relates to 1,2,4-substituted azetidine compounds and their use as antibacterial agents. This patent, we believe, gives us comprehensive intellectual property protection for our primary chemical modification.



## EXPERIMENTAL SECTION

**Chemistry at GIBH.** All commercially available solvents and reagents were purchased and used without further purification. All reactions were monitored by thin layer chromatography (TLC) with silica gel-coated plates and were visualized under UV light at 254 nm or by potassium permanganate solution staining followed by heating.  $^1\text{H}$  NMR spectra were acquired via a Bruker AVIII300 or AVIII400 at 300 or 400 MHz, respectively, at room temperature (21 to 28 °C).  $^{13}\text{C}$  NMR spectra were recorded via a Bruker AVIII400 or AVIII500 at 101 or 126 MHz, respectively, at room temperature.  $^{19}\text{F}$  NMR spectra were recorded via a Bruker AVIII500 at 471 MHz at room temperature. Chemical shifts ( $\delta$ ) are reported in parts per million relatives to residual solvent for  $^1\text{H}$  and  $^{13}\text{C}$  NMR spectroscopy. The NMR spectral data collected thus were processed using the MestReNova-12.0.3 software package. Coupling constants ( $J$ ) are reported in Hertz (Hz). Multiplicities of the signals are abbreviated as singlet (s), doublet (d), triplet (t), quartet (q), septet (sept), multiplet (m), and broad (br). Mass spectra were obtained on an API 2000 electrospray mass spectrometer. Infrared spectra were recorded at room temperature using a Bruker Tensor 27 FT-IR spectrometer using KBr pellets. Column chromatography purification was done using Silica Gel 200–300. Thin layer chromatography (TLC) was performed using aluminum-backed, F254-coated analytical TLC plates, which were visualized under UV light at 254 nm or by staining phosphomolybdic acid (in ethanol), followed by heating. Analytical HPLC was performed with an Agilent 1200 Series system using a Waters Acquity UPLC BEH 250  $\times$  4.6 mm, C18, 5  $\mu\text{m}$  column (solvent: MeOH-water +0.1%  $\text{NH}_3\text{H}_2\text{O}$ ; gradient: 1 mL  $\text{min}^{-1}$ ;  $T = 25^\circ\text{C}$ ) and UV detection at 210 nm wavelength. Purities for compounds BGaz-001–BGaz-005 were >95%.

**Synthesis of BGaz-001–BGaz-005.** Novel racemic 2,4-cis-amino-azetidine derivatives (BGaz-001–BGaz-005) were prepared and purified according to procedures reported for the synthesis of related compounds; for details, see Scheme S1.<sup>17–20</sup> Briefly, commercially available aldehydes (S1) and amines (S2) were dissolved in methanol and heated at reflux to afford the corresponding imines (S3).<sup>68–70</sup> Imines (S3) were isolated and subsequently reacted with *in situ* prepared allyl zinc reagent to afford homoallyl amine derivatives thereof (S4). The homoallyl amine derivatives (S4) thus obtained were dissolved in acetonitrile and treated with iodine (3 equiv) and sodium bicarbonate (5 equiv) at temperatures not exceeding 20 °C, resulting in cyclization to the corresponding 2-iodomethyl azetidine derivatives (S5). Displacement of iodine in derivatives S5 by the appropriate primary or secondary amines delivered the BGaz series of compounds in four linear steps.

**Bacterial Strains and Growth Conditions.** *M. smegmatis* mc<sup>2</sup>(2)155 was cultured at 37 °C, 180 rpm in Middlebrook 7H9 media supplemented with 0.05% Tween-80 or grown on LB agar. *M. bovis* BCG (strainTice) was cultured at 37 °C and 5%  $\text{CO}_2$ , static, in Middlebrook 7H9 media supplemented with 0.05% Tween-80 and 10% (v/v) BBL Middlebrook OADC enrichment or grown on Middlebrook 7H11 agar supplemented with 10% (v/v) BBL Middlebrook OADC enrichment.

**Determination of MIC and MBC.** The minimum inhibitory concentration ( $\text{MIC}_{99}$ ) was determined in 96-well flat bottom, black polystyrene microtiter plates (Greiner) in a final volume of 200  $\mu\text{L}$ . Compounds were two-fold serially diluted in neat DMSO and added to the microtiter plate at a final concentration of 1% DMSO. DMSO (1% in 7H9) was used as a negative control and rifampicin as a positive. The inoculum was standardized at OD<sub>600</sub> 0.05 in Middlebrook 7H9 medium and added to the plate, which was then incubated without shaking at 37 °C for 24 h (*M. smegmatis*)<sup>84</sup> or 7 days (*M. bovis* BCG). Following incubation, 42  $\mu\text{L}$  of resazurin (0.02% v/v in dH<sub>2</sub>O) was added to each well and incubated for a further 2 h (*M. smegmatis*) or 24 h (*M. bovis* BCG). Fluorescence was measured (Polar star omega plate reader ex 544 nm, em 590 nm), and the data were normalized using equation one. The concentration of the drug required to inhibit cell growth by 99% was calculated by

nonlinear regression (Gomperz equation for MIC determination, GraphPad Prism).

$$\left( \frac{x - \bar{x}(\text{negative controls})}{\bar{x}(\text{positive controls}) - \bar{x}(\text{negative controls})} \right) \times 100 \quad (1)$$

To determine the minimum bactericidal concentration (MBC), *M. smegmatis* and *M. bovis* BCG were grown in the presence of a two-fold serial dilution of the compound as mentioned above. After a 24-h (*M. smegmatis*) or 7-day (*M. bovis* BCG) incubation, the cells were pelleted and washed with phosphate buffered saline (PBS) pH 7.2. The washed cells were plated onto agar, devoid of compound, and incubated for 4 days (*M. smegmatis*) or 21 to 28 days *M. bovis* (BCG). The MBC was defined as the lowest concentration of compound, for which there was a 99% decrease of live bacteria compared with the inoculated amount.

**Determination of  $\text{MIC}_{\text{lux50}}$  against Autoluminescent *M.tb* H37Ra.** AlRa<sup>71</sup> (*Mtb* H37Ra::pTYOK) was homogenized with sterile glass beads in a 50 mL tube containing Middlebrook 7H9 medium (5 mL) plus 0.05% Tween 80, 10% v/v oleic acid albumin dextrose catalase (OADC) supplement (7H9-OADC-Tw). When OD<sub>600</sub> reached 0.3–0.5, relative light unit (RLU) counts were determined by placing culture (200  $\mu\text{L}$ ) on the detection hole of the luminometer. When the RLU reached 2 million/mL, the activities of compounds were assessed over a range of 3-fold increasing from 0.000001 to 10  $\mu\text{g/mL}$  prepared in 25  $\mu\text{L}$  AlRa broth culture (RLU diluted to 2000–4000/25  $\mu\text{L}$ ) grown in 7H9 broth without Tween 80. DMSO was used as negative control and isoniazid (INH, 10, 1, and 0.1  $\mu\text{g/mL}$ ) and rifampicin (RIF, 10, 1, and 0.1  $\mu\text{g/mL}$ ) were used as positive controls. RLU counts were determined four times daily (daily, i.e., days 0, 1, 2, and 3). The  $\text{MIC}_{\text{lux50}}$  was defined as determined as the lowest concentration that can inhibit >50% RLU compared with that from the untreated controls on day 3.<sup>72</sup>

**Determination of  $\text{MIC}_{99}$  for Clinical *M.tb* Strains.** The previously described resazurin microtiter assay (REMA) plate method was used.<sup>73,74</sup> Compounds were two-fold serially diluted in CAMR Mycobacterium Medium MOD2 (CMM MOD2).<sup>75</sup> Individual wells, in a 96-well plate, were inoculated with  $1 \times 10^6$  CFU  $\text{mL}^{-1}$  bacilli and incubated for 7 days at 37 °C with agitation (200 rpm). Following this, resazurin solution was added to wells (0.02% (w/v) in PBS pH 7.4, supplemented with 5% Tween 80).<sup>76</sup> The 96-well plates were incubated at room temperature for 6 h. The OD<sub>570nm</sub> of each well was recorded using a Tecan Sunrise plate reader. The minimum inhibitory concentration ( $\text{MIC}_{99}$ ) was calculated using a modified Gompertz function.<sup>77</sup> The optical density measurements for each drug concentration were compared to vehicle control to determine the percentage reduction in bacterial optical density.

**Physiochemical and Toxicological Analysis. Kinetic Solubility.** Compounds were solubilized (10 mM in DMSO) and diluted in PBS (pH 7.4) into a seven-point curve (0.2–100  $\mu\text{M}$ ) and incubated for 5 min at 25 °C with shaking (final DMSO concentration 1%). The turbidimetry was assessed at each of the seven concentrations using UV spectrophotometry at 620 nm, and the LogS was converted into the estimated solubility ( $S$ ) using the equation  $S = 10^{\text{LogS}}$ . Nicardipine hydrochloride was used as a control compound. All experiments were performed in triplicate.

**Mouse PPB.** Compounds were solubilized (10 mM in DMSO), and rapid equilibrium dialysis (RED) was used to measure the percentage binding to mouse plasma protein of the BGaz compounds at a final concentration of 5  $\mu\text{M}$ . The BGaz compound was incubated in 100% mouse plasma and dialyzed against buffer in a RED device for 4 h at 37 °C in a 5%  $\text{CO}_2$  incubator, with continuous shaking at 200 rpm. Samples were matrix-matched and analyzed by LC-MS/MS against a six-point standard curve prepared with 100% plasma. All experiments were performed in triplicate.

**Mouse Microsomal Clearance.** Compounds were solubilized (10 mM in DMSO). 1  $\mu\text{M}$  of BGaz compound was incubated with 0.5 mg/mL mouse microsomes in the presence or absence of the Phase 1 cofactor NADPH (1 mM) at 37 °C for 0, 5, 10, 15, and 30 min. The disappearance of the BGaz compound was assessed by LC-MS/MS.

All experiments were performed with two replicates per compound and were validated by the inclusion of up to three species-specific control compounds. Data output consists of mean intrinsic clearance ( $CL_{int}$ ) and half-life ( $t_{1/2}$ ) measurements.

**Mouse Hepatocyte Clearance.** Compounds were solubilized (10 mM in DMSO). 1  $\mu$ M of BGaz compound was incubated with  $0.5 \times 10^6$  cells/mL mouse hepatocytes at 37 °C for 0, 10, 20, 30, 45, and 60 min. The disappearance of the BGaz compound in the presence and absence of hepatocytes was assessed using LC-MS/MS. All experiments were performed with two replicates per compound and were validated by the inclusion of up to three species-specific control compounds. Data output consists of mean intrinsic clearance ( $CL_{int}$ ) and half-life ( $t_{1/2}$ ) measurements.

**Caco-2 and Efflux.** Compounds were solubilized (10 mM in DMSO), and the CacoReady Kit from ReadyCell S.L. (Barcelona, Spain) was used to determine compound permeability. Differentiated and polarized Caco-2 cells (21-day system) were plated on a 96-transwell permeable system as a single monolayer to allow for automated high throughput screening of compounds, and 10  $\mu$ M BGaz compound was added to the system in HBSS buffer (pH 7.4) and incubated for 2 h at 37 °C in a CO<sub>2</sub> incubator. Lucifer yellow was used as a cell monolayer integrity marker. Drug transport was assessed in both directions [apical to basolateral (A-B) and basolateral to apical (B-A)] across the cell monolayer. The buffer used for the assay does not include HEPES, so as to minimize the inhibitory effect on uptake transporters.<sup>78</sup> The BGaz compound concentrations were quantified using a calibration curve following analysis by LC-MS/MS, and the apparent permeability coefficient ( $P_{app}$ ) and efflux ratio of the compound across the monolayer were calculated. The efflux ratio is used as an indicator of active efflux. The permeability coefficient ( $P_{app}$ ) was calculated from the following equation:

$$P_{app} = \left( \frac{dQ/dt}{C_0 \times A} \right) \quad (2)$$

where  $dQ/dt$  is the amount of compound in the basal (A-B) or apical (B-A) compartment as a function of time (nmol/s).  $C_0$  is the initial concentration in the donor (apical or basal) compartment (Mean of  $T = 0$ ) (nmol/mL) and  $A$  is the area of the transwell (cm<sup>2</sup>).

The efflux ratio was then calculated as

$$\frac{P_{app}(B \text{ to } A)}{P_{app}(A \text{ to } B)} \quad (3)$$

All experiments were performed in triplicate, and the MDRI efflux markers Digoxin, quinidine, and propranolol were used as positive controls.

**Pharmacokinetic Studies.** Methods for combined single dosing (BGaz001–005) and dosing of single compounds multiple times (BGaz004 and BGaz005) are described in detail in the Supporting Information (PK Data).

**Cytochrome P450 Activities.** Compounds were solubilized to 10 mM in DMSO. The BGaz compounds were incubated at concentrations of 0.003, 0.009, 0.03, 0.08, 0.25, 0.74, 2.2, 6.7, and 20  $\mu$ M with CYP1A2, CYP2C9, CYP2C19, and CYP2D6 at 37 °C in the presence of the drug-like probe substrate HLM the Phase 1 cofactor NADPH (1 mM). The formation of metabolites of the drug-like probe substrates in the absence and presence of the BGaz compound was monitored by LC-MS/MS, and the  $IC_{50}$  value was determined. All assays had two replicates per compound and included a positive control inhibitor.

**HepG2 Mitochondrial Dysfunction.** Compounds were solubilized to 30 mM in DMSO. The BGaz compounds were added to the HepG2 cell model in a 96-well microplate in half log dilutions from 100–0.0003  $\mu$ M (final DMSO concentration 0.3%) using both glucose (DMEM consisting of 25 mM glucose) and galactose (DMEM consisting of 10 mM galactose) media. The compounds were incubated with the cell line for 24 h at 37 °C in a humidified CO<sub>2</sub> tissue culture incubator, followed by cell viability staining with MTT (3-(4,5-dimethylthiazol-2-yl)-2,5-diphenyltetrazolium bromide)

conversion to the Formazan product, determined by absorbance measurement. The cell viability  $IC_{50}$  was determined in HepG2 glucose and metabolism-modified HepG2 galactose, and the fold change difference between the Glu/Gal  $IC_{50}$  was determined. All experiments were performed in duplicate with the mitochondrial toxicity controls rotenone and Antimycin A and the cytotoxin control tamoxifen.

**hERG Cardiotoxicity Function.** Compounds were solubilized to 30 mM in DMSO before dilution in PBS to 300 mM. A further 3-fold on-board dilution resulted in a final top BGaz compound concentration of 100 mM. Eight-point concentration–response curves were generated using 3.16-fold serial dilutions from the top test concentration. Electrophysiological recordings were made from a Chinese Hamster Ovary cell line stably expressing the full length hERG channel. Single cell ionic currents were measured in the perforated patch clamp configuration (100  $\mu$ g mL<sup>−1</sup> amphotericin) at room temperature (21–23 °C) using an IonWorks Quattro instrument (Molecular Devices). The internal solution contained (mM) 140 KCl, 1 MgCl<sub>2</sub>, 1 EGTA, and 20 HEPES and was buffered to pH 7.3. The external solution [PBS contained (mM): 138 NaCl, 2.7 KCl, 0.9 CaCl<sub>2</sub>, 0.5 MgCl<sub>2</sub>, 8 Na<sub>2</sub>HPO<sub>4</sub>, and 1.5 KH<sub>2</sub>PO<sub>4</sub> buffered to pH 7.4]. Cells were clamped at a holding potential of −70 mV for 30 s and then stepped to +40 mV for one second. This was followed by a hyperpolarising step of 1 s to −30 mV to evoke the hERG tail current. Currents were measured from the tail step and referenced to the holding current. Compounds were then incubated for 3–4 min prior to a second measurement of the hERG signal using an identical pulsetrain.

**Mycobacterial Time Kill Experiments.** BGaz-004, BGaz-005, and isoniazid were 2-fold serially diluted in 100  $\mu$ L of CMM MOD2 medium from 96–3  $\mu$ M, 96–3  $\mu$ M, and 29.2–0.9  $\mu$ M; vehicle control (0.1% DMSO) was included in all experiments. Individual wells of a 96-well microtiter plate were inoculated to a starting bacterial titer of  $1 \times 10^6$  CFU mL<sup>−1</sup>. Microtiter plates were incubated for 0, 2, 6, 10, and 14 days at 37 °C with agitation (200 rpm). The bacterial titer at each time point was enumerated via outgrowth of bacilli on solid media for 3 weeks at 37 °C via a method adapted from Miles and Misra,<sup>27</sup> where triplicate 20  $\mu$ L spots of bacterial culture are spotted onto Middlebrook 7H10 agar for each 10-fold serial dilution. Statistical analyses of data were performed using a factorial ANOVA and posthoc Tukey's honestly significant difference test.

**Bacterial Staining and Flow Cytometry Analyses.** The method reported by Hendon-Dunn et al.<sup>28</sup> was used to analyze stained cell populations by flow cytometry. 100  $\mu$ L of *M. tuberculosis* H37Rv from each antibiotic incubation, at each time point, was transferred to a microtiter plate in quadruplicate and incubated in the dark for 1 h at 37 °C with either no dye added, 20  $\mu$ M calcein violet (CV-AM), 20  $\mu$ M sytox green (SG), or both 20  $\mu$ M CV-AM and 20  $\mu$ M SG. These incubations were then spun by centrifugation, and the supernatant was removed. The cells were fixed with 4% formaldehyde (v/v in water) for 1 h. The stained bacteria were examined using a Cytotflex S (Beckman Coulter) flow cytometer. Lasers with excitatory wavelengths of 488 and 405 nm were used. SG fluorescence emission (excitation and emission, 488 and 523 nm, respectively) was detected in the FIT-C channel (530/40 BP), and CV-AM fluorescence (excitation and emission, 400 and 452 nm, respectively) was detected in the PB-450 channel (450/50 BP). A quadrant gating strategy was used;<sup>28</sup> briefly, 10,000 single-cell events were gated upon using a two-parameter dot plot of forward scatter height versus forward scatter area. From gated single cells, the percentages of the total cell population residing in each polygonal population gate (P1: CV-AM<sup>−</sup>/SG<sup>−</sup>, P2: CV-AM<sup>+</sup>/SG<sup>−</sup>, P3: CV-AM<sup>+</sup>/SG<sup>+</sup>, P4: CV-AM<sup>−</sup>/SG<sup>+</sup>) were obtained. Statistical analysis of data was performed using a Student's *t*-test.

**Inhibition of Macromolecular Synthesis.** Inhibition of macromolecular biosynthesis was assayed by measuring the incorporation of radiolabeled precursors into DNA, RNA, protein, peptidoglycan, and fatty acids in the 10% trichloroacetic acid (TCA) extracts of cells exposed to azetidines. *M. smegmatis* were cultured in 7H9 media supplemented with 0.05% Tween-80 and grown to an OD<sub>600</sub> of 0.4.



Cultures (5 mL) were then transferred into sterile glass tubes and preincubated with 0×, 0.5×, 0.75× and 1 × MIC<sub>99</sub> azetidinones for 1 h at 37 °C with shaking. After preincubation, 10 μL of 500 nCi/μL [methyl-<sup>3</sup>H]thymidine, 500 nCi/μL [5,6-<sup>3</sup>H]uridine, 500 nCi/μL L-[4,5-<sup>3</sup>H]leucine, 500 nCi/μL [<sup>3</sup>H]meso-diaminopimelic acid, and 500 nCi/μL [<sup>14</sup>C]acetic acid were added to cultures to measure synthesis of DNA, RNA, protein, peptidoglycan and lipids, respectively. All cultures were incubated for 36 h, and 100 μL samples were sacrificed at 6, 12, 24, and 36 h time points by the addition of 50 μL 30%TCA/70% ethanol in Eppendorf tubes. Tubes were incubated at room temperature for 60 min to allow for precipitation of macromolecular material. Samples were individually vacuum filtered using 0.025 μm membrane filters (VSWP01300, MF-Millipore) that were prewashed with 500 μL 70% ethanol. Samples were washed with 3 × 500 μL 5% TCA, followed by 2 × 95% ethanol. Filter papers were dried and combined with 5 mL of scintillation fluid before measuring radioactive counts.

**Transcriptomic Profiling by RNA-seq Analysis.** *M. bovis* BCG was cultured to an OD<sub>600</sub> of 0.4 before exposure to 1 × MIC<sub>99</sub> concentrations of BGaz-004 or BGaz-005 for 8 h in three biological replicates and then compared to carrier control-treated bacilli. Cells were pelleted, flash-frozen in liquid nitrogen, and stored at −80 °C. Pellets were resuspended in lysozyme (600 μL, 5 mg/mL) and β-mercaptoethanol (7 μL/mL) in TE buffer and lysed by bead beating at 6 m/min (1 × 45 s). Samples were subjected to further bead beating (3 × 45 s), following the addition of (60 μL, 10% SDS). Sodium acetate pH 5.2 (3 M, 60 μL) and acidified phenol pH 4.2 (726 μL) were added, and the tubes were mixed well by inversion. Samples were incubated at 65 °C for 5 min and centrifuged for 5 min at 18,000 × g. The upper aqueous phase was transferred to a fresh tube, and an equal volume of acid phenol pH 4.2 was added and mixed well by inversion. Following heating (65 °C for 2 min) and centrifugation (5 min at 18,000 × g), the upper aqueous phase was once more transferred to a fresh tube, and an equal volume of chloroform:isoamyl alcohol (24:1 v/v) was added. The sample was mixed well by inversion and centrifuged at 18,000 × g for 5 min. The upper aqueous phase was transferred to a fresh tube, and a 1/10 volume of sodium acetate (3 M, pH 5.2) and three volumes of 100% ethanol were added. Samples were incubated at −20 °C overnight, centrifuged for 10 min (4 °C, 14,000 × g), and the supernatant removed. Ethanol (70% in water, 500 μL) was added to the pellet and centrifuged for 10 min (4 °C, 14,000 × g). The supernatant was removed, the pellet air-dried, and the extracted RNA resuspended in of RNase-free dH<sub>2</sub>O (40 μL). DNase treatment was performed using the TURBO DNA-free kit (Invitrogen). Briefly, a 0.1 × volume of 10 × TURBO DNase buffer was added to the RNA, along with TURBO DNase enzyme (1 μL of enzyme stock). The sample was incubated for 30 min at 37 °C, an additional TURBO DNase enzyme (1 μL of enzyme) was added, and the sample was incubated for another 30 min. DNase inactivation reagent (0.2 volumes) was added, and the sample was incubated at room temperature for 5 min. Following centrifugation at 10,000 × g for 1.5 min, the supernatant containing the RNA was transferred to a fresh tube and stored at −80 °C. The purified RNA was quantified, depleted of rRNA, and library-prepped before sequencing by Illumina HiSeq (150 × 2 paired end) by Genewiz Ltd. Adapter sequences and poor-quality reads were removed using Trimmomatic v.0.36, before mapping to the *Mycobacterium bovis* BCG Pasteur 1173P2 genome using Bowtie2 aligner v.2.2.6. Gene expression was quantified using FeatureCounts from the Subread package v.1.5.2. Differentially expressed genes were identified with the DESeq2 R package, normalized by the RLE method, and using the Wald test with Benjamini and Hochberg multiple testing correction. Genes with an adjusted *p*-value <0.05 and log<sub>2</sub> fold change >1 were considered to be differentially expressed. Significantly enriched signatures, with updated genome annotation,<sup>79,80</sup> were identified using the hypergeometric function comparing to published drug responses<sup>41,42</sup> or mapped to metabolic pathways.<sup>35,36</sup> Genes significantly differentially expressed in response to BGaz-004 and BGaz-005 are detailed in Supporting Information.

Fully annotated RNA-seq data will be deposited in ArrayExpress; the accession number will be provided.

**Radioisotope Labeling of Lipids and Analysis.** Cells were grown to an OD<sub>600</sub> 0.5, treated with compound, and grown for 6 h (*M. smegmatis*) or overnight (*M. bovis* BCG). For radio labeling experiments, 1 μCi mL<sup>−1</sup> <sup>14</sup>C acetic acid was then added, followed by a 16-h incubation. Cells were harvested and extracted using chloroform:methanol:water (10:10:3, v/v/v, 2 mL) for 2 h at 50 °C. Following centrifugation, the organic extracts were combined with chloroform and water (1.75 and 0.75 mL respectively). The lower organic phase containing associated lipids was recovered, washed twice with chloroform:methanol:water (3:47:48, v/v/v, 2 mL), and dried with nitrogen gas. Samples were resuspended in chloroform:methanol (2:1, v/v, 200 μL), and OD-adjusted volumes were subjected to thin-layer chromatography (TLC) analysis. Cell wall-associated lipids were visualized by either heating TLC plates after treatment with molybdophosphoric acid (MPA) in ethanol (5% w/v) or alpha-naphthol in ethanol (5% w/v), or by autoradiography by exposure to Kodak BioMax MR film.

Cell wall-bound lipids from the delipidated extracts from the abovementioned extraction were released by the addition of a solution of tetra-butyl ammonium hydroxide (TBAH) (5% m/v, 2 mL), followed by a 16-h incubation at 100 °C. Water (2 mL), dichloromethane (4 mL), and iodomethane (200 μL) were then added and mixed thoroughly for 30 min. The organic phase was recovered, following centrifugation, and washed with water (3 × 4 mL), dried, and resuspended in diethyl ether (4 mL). After sonication and centrifugation, the supernatant was dried and resuspended in dichloromethane. Equivalent aliquots of the samples were subjected to TLC in petroleum ether:acetone (95:5, v/v) and visualized by MPA and heat or autoradiography.

**Target Gene Overexpression Studies.** The constructs pMV261\_mmpL3 and pVV16\_trpAB,<sup>50,81</sup> including the empty pMV261 and pVV16 vectors, were electroporated into *M. bovis* BCG as previously described, and the MIC<sub>99</sub> determined as described above. The constructs pTIC6\_fbpA, pTIC6\_fbpB, and pTIC6\_fbpC were synthesized by GenScript Ltd. by inserting the coding regions of the *M. tuberculosis* H37Rv genes into the vector pTIC6, which encodes kanamycin selection. The constructs and empty pTIC6 vector were electroporated into *M. bovis* BCG. Following induction of gene expression with 50 ng/mL of anhydrotetracycline for 24 h, the MIC<sub>99</sub> was determined as described above.

## ■ ASSOCIATED CONTENT

### SI Supporting Information

The Supporting Information is available free of charge at <https://pubs.acs.org/doi/10.1021/acs.jmedchem.3c01643>.

Supplementary PK data (PDF).

A detailed description of author contributions, general methods, chemical and biological general procedures, synthetic chemistry protocols for the synthesis of BGaz001–BGaz0016, NMR spectra, details of mass spectrometry analysis, additional corresponding references,<sup>82,83</sup> and molecular formula strings (ZIP).

## ■ AUTHOR INFORMATION

### Corresponding Authors

Luke Alderwick – Institute of Microbiology and Infection, School of Biosciences, University of Birmingham, Birmingham, West Midlands B15 2TT, U.K.; Discovery Sciences, Charles River Laboratories, Saffron Walden CB10 1XL, U.K.; [orcid.org/0000-0002-1257-6053](https://orcid.org/0000-0002-1257-6053); Email: [luke.alderwick@crl.com](mailto:luke.alderwick@crl.com)

John S. Fossey – School of Chemistry, University of Birmingham, Birmingham, West Midlands B15 2TT, U.K.;

orcid.org/0000-0002-2626-5117; Email: j.s.fossey@bham.ac.uk

**Cleopatra Neagoie** – State Key Laboratory of Respiratory Disease, China-New Zealand Joint Laboratory on Biomedicine and Health, Guangzhou Institutes of Biomedicine and Health, Chinese Academy of Science, Guangzhou 510530, China; Centre for Regenerative Medicine and Health, Hong Kong Institute of Science & Innovation, Chinese Academy of Sciences, NT, Hong Kong SAR; Visiting Scientist, School of Chemistry, University of Birmingham, Birmingham, West Midlands B15 2TT, U.K.; orcid.org/0000-0003-2289-3949; Email: cleopatra.neagoie@crmh-cas.org.hk

## Authors

**Yixin Cui** – School of Chemistry, University of Birmingham, Birmingham, West Midlands B15 2TT, U.K.

**Alice Lanne** – Institute of Microbiology and Infection, School of Biosciences, University of Birmingham, Birmingham, West Midlands B15 2TT, U.K.

**Xudan Peng** – State Key Laboratory of Respiratory Disease, China-New Zealand Joint Laboratory on Biomedicine and Health, Guangzhou Institutes of Biomedicine and Health, Chinese Academy of Science, Guangzhou 510530, China

**Edward Browne** – Sygnature Discovery, Nottingham NG1 1GR, U.K.

**Apoorva Bhatt** – Institute of Microbiology and Infection, School of Biosciences, University of Birmingham, Birmingham, West Midlands B15 2TT, U.K.

**Nicholas J. Colman** – School of Biosciences, University of Birmingham, Birmingham, West Midlands B15 2TT, U.K.; orcid.org/0000-0002-8210-9178

**Philip Craven** – School of Chemistry, University of Birmingham, Birmingham, West Midlands B15 2TT, U.K.; orcid.org/0000-0002-7617-132X

**Liam R. Cox** – School of Chemistry, University of Birmingham, Birmingham, West Midlands B15 2TT, U.K.; orcid.org/0000-0001-7018-3904

**Nicholas J. Cundy** – School of Chemistry, University of Birmingham, Birmingham, West Midlands B15 2TT, U.K.; orcid.org/0000-0001-6783-5422

**Katie Dale** – Institute of Microbiology and Infection, School of Biosciences, University of Birmingham, Birmingham, West Midlands B15 2TT, U.K.

**Antonio Feula** – School of Chemistry, University of Birmingham, Birmingham, West Midlands B15 2TT, U.K.

**Jon Frampton** – College of Medical and Dental Sciences, University of Birmingham, Birmingham, West Midlands B15 2TT, U.K.

**Martin Fung** – Centre for Regenerative Medicine and Health, Hong Kong Institute of Science & Innovation, Chinese Academy of Sciences, NT, Hong Kong SAR

**Michael Morton** – ApconiX Ltd, Cheshire SK10 4TG, U.K.

**Aaron Goff** – Department of Global Health and Infection, Brighton and Sussex Medical School, University of Sussex, Falmer BN1 9PX, U.K.

**Mariwan Salih** – School of Chemistry, University of Birmingham, Birmingham, West Midlands B15 2TT, U.K.

**Xingfen Lang** – State Key Laboratory of Respiratory Disease, China-New Zealand Joint Laboratory on Biomedicine and Health, Guangzhou Institutes of Biomedicine and Health, Chinese Academy of Science, Guangzhou 510530, China

**Xingjian Li** – School of Chemistry, University of Birmingham, Birmingham, West Midlands B15 2TT, U.K.; State Key Laboratory of Respiratory Disease, China-New Zealand Joint Laboratory on Biomedicine and Health, Guangzhou Institutes of Biomedicine and Health, Chinese Academy of Science, Guangzhou 510530, China

**Chris Moon** – TB Research Group, National Infection Service, Public Health England (UKHSA), Salisbury SP4 0JG, U.K.

**Jordan Pascoe** – TB Research Group, National Infection Service, Public Health England (UKHSA), Salisbury SP4 0JG, U.K.

**Vanessa Portman** – Sygnature Discovery, Nottingham NG1 1GR, U.K.

**Cara Press** – Institute of Microbiology and Infection, School of Biosciences, University of Birmingham, Birmingham, West Midlands B15 2TT, U.K.

**Timothy Schulz-Utermoehl** – Sygnature Discovery, Nottingham NG1 1GR, U.K.

**Suki Lee** – Centre for Regenerative Medicine and Health, Hong Kong Institute of Science & Innovation, Chinese Academy of Sciences, NT, Hong Kong SAR

**Micky D. Tortorella** – State Key Laboratory of Respiratory Disease, China-New Zealand Joint Laboratory on Biomedicine and Health, Guangzhou Institutes of Biomedicine and Health, Chinese Academy of Science, Guangzhou 510530, China; Centre for Regenerative Medicine and Health, Hong Kong Institute of Science & Innovation, Chinese Academy of Sciences, NT, Hong Kong SAR

**Zhengchao Tu** – State Key Laboratory of Respiratory Disease, China-New Zealand Joint Laboratory on Biomedicine and Health, Guangzhou Institutes of Biomedicine and Health, Chinese Academy of Science, Guangzhou 510530, China

**Zoe E. Underwood** – TB Research Group, National Infection Service, Public Health England (UKHSA), Salisbury SP4 0JG, U.K.; orcid.org/0000-0002-4777-5757

**Changwei Wang** – State Key Laboratory of Respiratory Disease, China-New Zealand Joint Laboratory on Biomedicine and Health, Guangzhou Institutes of Biomedicine and Health, Chinese Academy of Science, Guangzhou 510530, China

**Akina Yoshizawa** – School of Chemistry, University of Birmingham, Birmingham, West Midlands B15 2TT, U.K.

**Tianyu Zhang** – State Key Laboratory of Respiratory Disease, China-New Zealand Joint Laboratory on Biomedicine and Health, Guangzhou Institutes of Biomedicine and Health, Chinese Academy of Science, Guangzhou 510530, China; orcid.org/0000-0001-5647-6014

**Simon J. Waddell** – Department of Global Health and Infection, Brighton and Sussex Medical School, University of Sussex, Falmer BN1 9PX, U.K.; orcid.org/0000-0002-3684-9116

**Joanna Bacon** – TB Research Group, National Infection Service, Public Health England (UKHSA), Salisbury SP4 0JG, U.K.

Complete contact information is available at:

<https://pubs.acs.org/10.1021/acs.jmedchem.3c01643>

## Author Contributions

C.N. and L.A. share joint last authorship together with J.S.F.; Y.C. and A.L. share joint first authorship. Contributions for all authors are described in the Supporting Information. C.N.:



Medicinal chemistry aspects including azetidine design; J.S.F.: synthetic chemistry aspects; L.A.: microbiology studies including compound MIC profiling, mode of action, and chemical profiling of mycobacterial phenotypes. Joint first authors: Y.C. contributed to the development of methodology for the synthesis of azetidine derivatives and transferred knowledge between teams. A.L. examined biological activity, determined MIC values, probed target/mechanism, and elucidated aspects of the mode of action; all the experimentation and analyses using *Mycobacterium tuberculosis* were performed by JB's team at PHE Porton (UKHSA). All authors contributed critically to devising and executing aspects of this research. A detailed and comprehensive description of author contributions is defined in the associated Supporting Information.

### Notes

The authors declare the following competing financial interest(s): A patent application disclosing aspects of this study has been filed by the University of Birmingham. The views expressed in this publication are those of the authors and not necessarily those of Public Health England (UKHSA), or the Department of Health. The authors declare no other competing interests.

### ACKNOWLEDGMENTS

We dedicate this study to the memory of Professor John Fossey, an exceptional synthetic chemist who passed away on April 15, 2022. Professor Fossey's passion for chirality and stereoselective synthesis marked him as a distinguished scientific leader in the field of chemistry. His legacy endures through his scientific integrity, innovative thinking, and his role as a remarkable scientific mentor and collaborator. Professor John Fossey will be profoundly missed by colleagues, family, and friends, and we extend our deepest sympathies and sincere condolences to his loved ones. We are grateful for the support underpinning much of this study from MRC Confidence in Concepts and EPSRC follow-on fund schemes. The University of Birmingham is acknowledged for support, including travel funds permitting A.Y., X.L., and Y.C. to undertake training placements at GIBH. J.S.F. is grateful to the Royal Society for the training provided because of a previous Industrial Fellowship and the EPSRC for previous funding (EP/J003220/1). Funding for part of this study was received from Public Health England. This work was supported by the National Key R&D Program of China (2021 YFA1300900) and by the Chinese Academy of Sciences Grant (YJ-KYYQ20210026, 154144KYSB20190005). S.J.W. and A.G. thank the National Centre for the Replacement, Refinement, and Reduction of Animals in Research (NC3Rs) for grant support (NC/R001669/1). Qiong Pan (GIBH), Jingfang Xiong (GIBH), and Miaoqin She (GIBH) are acknowledged for conducting aspects of the PK/PD studies of this report. Dr. Chi Tsang (UoB), Dr. Peter Ashton (UoB), and Jiajia Wei (GIBH) are acknowledged for their helpful discussions and practical support with aspects of mass spectrometry. Dr. Cécile S. Le Duff (UoB) and Dr. Neil Spencer (UoB) gave advice on aspects of NMR spectroscopy underpinning the preliminary or previously reported, findings. Yingxue Liu (GIBH) is acknowledged for help with the purification of final products by HPLC where required.

### ABBREVIATIONS USED

AG, Arabinogalactan; Ag85, antigen 85; BGaz, azetidine derivate; MmpL3, mycobacterial membrane protein Large 3; PKs13, polyketide synthase 13; TDM, trehalose dimycolate; TMM, trehalose monomycolate; WGS, whole genome sequencing.

### REFERENCES

- (1) [www.who.int/gho/tb/en/](http://www.who.int/gho/tb/en/). World Health Organisation: Global Health Observatory (GHO) data [www.who.int/gho/tb/en/](http://www.who.int/gho/tb/en/).
- (2) *Global tuberculosis report 2022*; World Health Organization: Geneva, 2022, Licence: CC BY-NC-SA 3.0 IGO.
- (3) Combs, D. L.; O'Brien, R. J.; Geiter, L. J. USPHS Tuberculosis Short-Course Chemotherapy Trial 21: Effectiveness, Toxicity, and Acceptability: The Report of Final Results. *Ann. Int. Med.* **1990**, *112*, 397–406.
- (4) Shah, N. S.; Wright, A.; Bai, G. H.; Barrera, L.; Boulahbal, F.; Martin-Casabona, N.; Drobniewski, F.; Gilpin, C.; Havelkova, M.; Lepe, R.; Lumb, R.; Metchock, B.; Portaels, F.; Rodrigues, M. F.; Rusch-Gerdes, S.; Van Deun, A.; Vincent, V.; Laserson, K.; Wells, C.; Cegielski, J. P. Worldwide emergence of extensively drug-resistant tuberculosis. *Emerg. Infect. Dis.* **2007**, *13*, 380–7.
- (5) Sharma, S. K.; Mohan, A. Multidrug-Resistant Tuberculosis: A Menace That Threatens To Destabilize Tuberculosis Control. *Chest* **2006**, *130*, 261–272.
- (6) Zumla, A.; Nahid, P.; Cole, S. T. Advances in the development of new tuberculosis drugs and treatment regimens. *Nat. Rev. Drug Discovery* **2013**, *12*, 388–404.
- (7) Ma, Z.; Lienhardt, C.; McIlleron, H.; Nunn, A. J.; Wang, X. Global tuberculosis drug development pipeline: the need and the reality. *Lancet* **2010**, *375*, 2100–2109.
- (8) Sharma, A.; De Rosa, M.; Singla, N.; Singh, G.; Barnwal, R. P.; Pandey, A. Tuberculosis: An Overview of the Immunogenic Response, Disease Progression, and Medicinal Chemistry Efforts in the Last Decade toward the Development of Potential Drugs for Extensively Drug-Resistant Tuberculosis Strains. *J. Med. Chem.* **2021**, *64*, 4359–4395.
- (9) Raymer, B.; Bhattacharya, S. K. Lead-like Drugs: A Perspective. *J. Med. Chem.* **2018**, *61*, 10375–10384.
- (10) Lovering, F. Escape from Flatland 2: complexity and promiscuity. *MedChemComm* **2013**, *4*, 515–519.
- (11) Lovering, F.; Bikker, J.; Humblet, C. Escape from Flatland: Increasing Saturation as an Approach to Improving Clinical Success. *J. Med. Chem.* **2009**, *52*, 6752–6756.
- (12) Yang, Y.; Chen, H.; Nilsson, I.; Muresan, S.; Engkvist, O. Investigation of the Relationship between Topology and Selectivity for Druglike Molecules. *J. Med. Chem.* **2010**, *53*, 7709–7714.
- (13) Baell, J. B.; Holloway, G. A. New Substructure Filters for Removal of Pan Assay Interference Compounds (PAINS) from Screening Libraries and for Their Exclusion in Bioassays. *J. Med. Chem.* **2010**, *53*, 2719–2740.
- (14) Baell, J. B.; Nissink, J. W. M. Seven Year Itch: Pan-Assay Interference Compounds (PAINS) in 2017—Utility and Limitations. *ACS Chem. Biol.* **2018**, *13*, 36–44.
- (15) Colomer, I.; Empson, C. J.; Craven, P.; Owen, Z.; Doveston, R. G.; Churcher, I.; Marsden, S. P.; Nelson, A. A divergent synthetic approach to diverse molecular scaffolds: assessment of lead-likeness using LLAMA, an open-access computational tool. *Chem. Commun.* **2016**, *52*, 7209–7212.
- (16) Synthetic chemistry methodology projects within the School of Chemistry at the University of Birmingham initially provided ~ 200 compounds suitable for biological screening.
- (17) Feula, A.; Dhillon, S. S.; Byravan, R.; Sangha, M.; Ebanks, R.; Hama Salih, M. A.; Spencer, N.; Male, L.; Magyary, I.; Deng, W.-P.; Müller, F.; Fossey, J. S. Synthesis of azetidines and pyrrolidines via iodocyclisation of homoallyl amines and exploration of activity in a zebrafish embryo assay. *Org. Biomol. Chem.* **2013**, *11*, 5083–5093.

- (18) Feula, A.; Male, L.; Fossey, J. S. Diastereoselective preparation of azetidines and pyrrolidines. *Org. Lett.* **2010**, *12*, 5044–5047.
- (19) Yoshizawa, A.; Feula, A.; Leach, A. G.; Male, L.; Fossey, J. S. Palladium and Platinum 2,4-*cis*-amino Azetidine and Related Complexes. *Front. Chem.* **2018**, *6*, 211.
- (20) Yoshizawa, A.; Feula, A.; Male, L.; Leach, A. G.; Fossey, J. S. Rigid and concave, 2,4-*cis*-substituted azetidine derivatives: A platform for asymmetric catalysis. *Sci. Rep.* **2018**, *8*, 6541.
- (21) [www.birmingham.ac.uk/facilities/bddf](http://www.birmingham.ac.uk/facilities/bddf). Birmingham Drug Discovery Facility. [www.birmingham.ac.uk/facilities/bddf](http://www.birmingham.ac.uk/facilities/bddf).
- (22) The synthesis and preliminary screening data of ~ 100 azetidine derivatives that were less active, and not investigated further, will be reported elsewhere.
- (23) Palomino, J.-C.; Martin, A.; Camacho, M.; Guerra, H.; Swings, J.; Portaels, F. Resazurin Microtiter Assay Plate: Simple and Inexpensive Method for Detection of Drug Resistance in *Mycobacterium tuberculosis*. *Antimicrob. Agents Chemother.* **2002**, *46*, 2720.
- (24) Yang, F.; Njire, M. M.; Liu, J.; Wu, T.; Wang, B.; Liu, T.; Cao, Y.; Liu, Z.; Wan, J.; Tu, Z.; Tan, Y.; Tan, S.; Zhang, T. Engineering more stable, selectable marker-free autoluminescent mycobacteria by one step. *PLoS One* **2015**, *10*, No. e0119341.
- (25) Qin, L.; Wang, J.; Lu, J.; Yang, H.; Zheng, R.; Liu, Z.; Huang, X.; Feng, Y.; Hu, Z.; Ge, B. A deletion in the RD105 region confers resistance to multiple drugs in *Mycobacterium tuberculosis*. *BMC Biol.* **2019**, *17*, 7.
- (26) Hoagland, D. T.; Liu, J.; Lee, R. B.; Lee, R. E. New agents for the treatment of drug-resistant *Mycobacterium tuberculosis*. *Adv. Drug Delivery Rev.* **2016**, *102*, 55–72.
- (27) Miles, A. A.; Misra, S. S.; Irwin, J. O. The estimation of the bactericidal power of the blood. *Epidemiol. Infect.* **1938**, *38*, 732–749.
- (28) Hendon-Dunn, C. L.; Doris, K. S.; Thomas, S. R.; Allnutt, J. C.; Marriott, A. A. N.; Hatch, K. A.; Watson, R. J.; Bottley, G.; Marsh, P. D.; Taylor, S. C.; Bacon, J. A Flow Cytometry Method for Rapidly Assessing *Mycobacterium tuberculosis* Responses to Antibiotics with Different Modes of Action. *Antimicrob. Agents Chemother.* **2016**, *60*, 3869.
- (29) Abrahams, K. A.; Cox, J. A. G.; Spivey, V. L.; Loman, N. J.; Pallen, M. J.; Constantinidou, C.; Fernandez, R.; Alemparte, C.; Remuinan, M. J.; Barros, D.; Ballell, L.; Besra, G. S. Identification of Novel Imidazo[1,2-*a*]pyridine Inhibitors Targeting *M. tuberculosis* QcrB. *PLoS One* **2012**, *7*, No. e52951. ARTN
- (30) Abrahams, K. A.; Chung, C.-W.; Ghidelli-Disse, S.; Rullas, J.; Rebollo-López, M. J.; Gurcha, S. S.; Cox, J. A. G.; Mendoza, A.; Jiménez-Navarro, E.; Martínez-Martínez, M. S.; Neu, M.; Shillings, A.; Homes, P.; Argyrou, A.; Casanueva, R.; Loman, N. J.; Moynihan, P. J.; Lelièvre, J.; Selenski, C.; Axtman, M.; Kremer, L.; Bantscheff, M.; Angulo-Barturen, I.; Izquierdo, M. C.; Cammack, N. C.; Drewes, G.; Ballell, L.; Barros, D.; Besra, G. S.; Bates, R. H. Identification of KasA as the cellular target of an anti-tubercular scaffold. *Nat. Commun.* **2016**, *7*, 12581.
- (31) Andries, K.; Verhasselt, P.; Guillemont, J.; Göhlmann, H. W. H.; Neefs, J.-M.; Winkler, H.; Van Gestel, J.; Timmerman, P.; Zhu, M.; Lee, E.; Williams, P.; de Chaffoy, D.; Huitric, E.; Hoffner, S.; Cambau, E.; Truffot-Pernot, C.; Lounis, N.; Jarlier, V. A Diarylquinoline Drug Active on the ATP Synthase of *Mycobacterium tuberculosis*. *Science* **2005**, *307*, 223.
- (32) Batt, S. M.; Cacho Izquierdo, M.; Castro Pichel, J.; Stubbs, C. J.; Vela-Glez Del Peral, L.; Pérez-Herrán, E.; Dhar, N.; Mouzon, B.; Rees, M.; Hutchinson, J. P.; Young, R. J.; McKinney, J. D.; Barros Aguirre, D.; Ballell, L.; Besra, G. S.; Argyrou, A. Whole Cell Target Engagement Identifies Novel Inhibitors of *Mycobacterium tuberculosis* Decaprenylphosphoryl- $\beta$ -D-ribose Oxidase. *ACS Infect. Dis.* **2015**, *1*, 615–626.
- (33) Manganelli, R.; Voskuil, M. I.; Schoolnik, G. K.; Smith, I. The *Mycobacterium tuberculosis* ECF sigma factor sigmaE: role in global gene expression and survival in macrophages. *Mol. Microbiol.* **2001**, *41*, 423–37.
- (34) Balazsi, G.; Heath, A. P.; Shi, L.; Gennaro, M. L. The temporal response of the *Mycobacterium tuberculosis* gene regulatory network during growth arrest. *Mol. Syst. Biol.* **2008**, *4*, 225.
- (35) Karp, P. D.; Billington, R.; Caspi, R.; Fulcher, C. A.; Latendresse, M.; Kothari, A.; Keseler, I. M.; Krummenacker, M.; Midford, P. E.; Ong, Q.; Ong, W. K.; Paley, S. M.; Subhraveti, P. The BioCyc collection of microbial genomes and metabolic pathways. *Brief. Bioinform.* **2019**, *20*, 1085–1093.
- (36) Caspi, R.; Billington, R.; Ferrer, L.; Foerster, H.; Fulcher, C. A.; Keseler, I. M.; Kothari, A.; Krummenacker, M.; Latendresse, M.; Mueller, L. A.; Ong, Q.; Paley, S.; Subhraveti, P.; Weaver, D. S.; Karp, P. D. The MetaCyc database of metabolic pathways and enzymes and the BioCyc collection of pathway/genome databases. *Nucleic Acids Res.* **2016**, *44*, D471–80.
- (37) Chang, Y.; Fox, B. G. Identification of Rv3230c as the NADPH oxidoreductase of a two-protein DesA3 acyl-CoA desaturase in *Mycobacterium tuberculosis* H37Rv. *Biochemistry* **2006**, *45*, 13476–86.
- (38) McGillivray, A.; Golden, N. A.; Gautam, U. S.; Mehra, S.; Kaushal, D. The *Mycobacterium tuberculosis* Rv2745c plays an important role in responding to redox stress. *PLoS One* **2014**, *9*, No. e93604.
- (39) Hards, K.; Robson, J. R.; Berney, M.; Shaw, L.; Bald, D.; Koul, A.; Andries, K.; Cook, G. M. Bactericidal mode of action of bedaquiline. *J. Antimicrob. Chemother.* **2015**, *70*, 2028–2037.
- (40) Mishra, S.; Shukla, P.; Bhaskar, A.; Anand, K.; Baloni, P.; Jha, R. K.; Mohan, A.; Rajmani, R. S.; Nagaraja, V.; Chandra, N.; Singh, A. Efficacy of  $\beta$ -lactam/ $\beta$ -lactamase inhibitor combination is linked to WhiB4-mediated changes in redox physiology of *Mycobacterium tuberculosis*. *eLife* **2017**, *6*, No. e25624.
- (41) Waddell, S. J.; Stabler, R. A.; Laing, K.; Kremer, L.; Reynolds, R. C.; Besra, G. S. The use of microarray analysis to determine the gene expression profiles of *Mycobacterium tuberculosis* in response to anti-bacterial compounds. *Tuberculosis* **2004**, *84*, 263–74.
- (42) Boshoff, H. I.; Myers, T. G.; Copp, B. R.; McNeil, M. R.; Wilson, M. A.; Barry, C. E., 3rd The transcriptional responses of *Mycobacterium tuberculosis* to inhibitors of metabolism: Novel insights into drug mechanisms of action. *J. Biol. Chem.* **2004**, *279*, 40174–84.
- (43) Amaral, L.; Viveiros, M. Thioridazine: A Non-Antibiotic Drug Highly Effective, in Combination with First Line Anti-Tuberculosis Drugs, against Any Form of Antibiotic Resistance of *Mycobacterium tuberculosis* Due to Its Multi-Mechanisms of Action. *Antibiotics* **2017**, *6*, 3.
- (44) Lee, R. E.; Protopopova, M.; Crooks, E.; Slayden, R. A.; Terrot, M.; Barry, C. E., 3rd Combinatorial lead optimization of [1,2]-diamines based on ethambutol as potential antituberculosis preclinical candidates. *J. Comb. Chem.* **2003**, *5*, 172–87.
- (45) Makarov, V.; Manina, G.; Mikusova, K.; Möllmann, U.; Ryabova, O.; Saint-Joanis, B.; Dhar, N.; Pasca, M. R.; Buroni, S.; Lucarelli, A. P.; Milano, A.; De Rossi, E.; Belanova, M.; Bobovska, A.; Dianiskova, P.; Kordulakova, J.; Sala, C.; Fullam, E.; Schneider, P.; McKinney, J. D.; Brodin, P.; Christophe, T.; Waddell, S.; Butcher, P.; Albrechtsen, J.; Rosenkrands, I.; Brosch, R.; Nandi, V.; Bharath, S.; Gaonkar, S.; Shandil, R. K.; Balasubramanian, V.; Balganes, T.; Tyagi, S.; Grosset, J.; Riccardi, G.; Cole, S. T. Benzothiazinones Kill *Mycobacterium tuberculosis* by Blocking Arabinan Synthesis. *Science* **2009**, *324*, 801.
- (46) Xu, Z.; Meshcheryakov, V. A.; Poce, G.; Chng, S.-S. MmpL3 is the flippase for mycolic acids in mycobacteria. *Proc. Natl. Acad. Sci. U.S.A.* **2017**, *114*, 7993.
- (47) Portevin, D.; de Sousa, D.; Auria, C.; Houssin, C.; Grimaldi, C.; Chami, M.; Daffé, M.; Guilhot, C. A polyketide synthase catalyzes the last condensation step of mycolic acid biosynthesis in mycobacteria and related organisms. *Proc. Natl. Acad. Sci. U. S. A.* **2004**, *101*, 314.
- (48) Gavalda, S.; Bardou, F.; Laval, F.; Bon, C.; Malaga, W.; Chalut, C.; Guilhot, C.; Mourey, L.; Daffé, M.; Quémard, A. The Polyketide Synthase Pks13 Catalyzes a Novel Mechanism of Lipid Transfer in *Mycobacteria*. *Chem. Biol.* **2014**, *21*, 1660–1669.
- (49) Su, C.-C.; Klenotic, P. A.; Bolla, J. R.; Purdy, G. E.; Robinson, C. V.; Yu, E. W. MmpL3 is a lipid transporter that binds trehalose



monomycolate and phosphatidylethanolamine. *Proc. Natl. Acad. Sci. U.S.A.* **2019**, *116*, 11241.

(50) Cox, J. A. G.; Abrahams, K. A.; Alemparte, C.; Ghidelli-Disse, S.; Rullas, J.; Angulo-Barturen, I.; Singh, A.; Gurcha, S. S.; Nataraj, V.; Bethell, S.; Remuñán, M. J.; Encinas, L.; Jervis, P. J.; Cammack, N. C.; Bhatt, A.; Kruse, U.; Bantscheff, M.; Fütterer, K.; Barros, D.; Ballell, L.; Drewes, G.; Besra, G. S. THPP target assignment reveals EchA6 as an essential fatty acid shuttle in mycobacteria. *Nat. Microbiol.* **2016**, *1*, 15006.

(51) Belisle, J. T.; Vissa, V. D.; Sievert, T.; Takayama, K.; Brennan, P. J.; Besra, G. S. Role of the Major Antigen of *Mycobacterium tuberculosis* in Cell Wall Biogenesis. *Science* **1997**, *276*, 1420.

(52) Favrot, L.; Grzegorzewicz, A. E.; Lajiness, D. H.; Marvin, R. K.; Boucau, J.; Isailovic, D.; Jackson, M.; Ronning, D. R. Mechanism of inhibition of *Mycobacterium tuberculosis* antigen 85 by eiselen. *Nat. Commun.* **2013**, *4*, 2748.

(53) Mdluli, K.; Kaneko, T.; Upton, A. The tuberculosis drug discovery and development pipeline and emerging drug targets. *Cold Spring Harb. Perspect. Med.* **2015**, *5*, a021154.

(54) Ling, L. L.; Schneider, T.; Peoples, A. J.; Spoering, A. L.; Engels, I.; Conlon, B. P.; Mueller, A.; Schäberle, T. F.; Hughes, D. E.; Epstein, S.; Jones, M.; Lazarides, L.; Steadman, V. A.; Cohen, D. R.; Felix, C. R.; Fetterman, K. A.; Millett, W. P.; Nitti, A. G.; Zullo, A. M.; Chen, C.; Lewis, K. A new antibiotic kills pathogens without detectable resistance. *Nature* **2015**, *517*, 455–459.

(55) Isoniazid was included as a positive control (0.9–29.2  $\mu\text{M}$ ), and comparison, with it being an antibiotic that targets the cell wall and has rapid bactericidal activity.

(56) Hendon-Dunn, C. L.; Pertinez, H.; Marriott, A. A. N.; Hatch, K. A.; Allnutt, J. C.; Davies, G.; Bacon, J. Regrowth of *Mycobacterium tuberculosis* Populations Exposed to Antibiotic Combinations Is Due to the Presence of Isoniazid and Not Bacterial Growth Rate. *Antimicrob. Agents Chemother.* **2019**, *63*, No. e00570-19.

(57) Banerjee, A.; Dubnau, E.; Quemard, A.; Balasubramanian, V.; Um, K. S.; Wilson, T.; Collins, D.; de Lisle, G.; Jacobs, W. R. inhA, a gene encoding a target for isoniazid and ethionamide in *Mycobacterium tuberculosis*. *Science* **1994**, *263*, 227.

(58) Takayama, K.; Kilburn, J. O. Inhibition of synthesis of arabinogalactan by ethambutol in *Mycobacterium smegmatis*. *Antimicrob. Agents Chemother.* **1989**, *33*, 1493.

(59) Tahlan, K.; Wilson, R.; Kastrinsky, D. B.; Arora, K.; Nair, V.; Fischer, E.; Barnes, S. W.; Walker, J. R.; Alland, D.; Barry, C. E.; Boshoff, H. I. SQ109 Targets MmpL3, a Membrane Transporter of Trehalose Monomycolate Involved in Mycolic Acid Donation to the Cell Wall Core of *Mycobacterium tuberculosis*. *Antimicrob. Agents Chemother.* **2012**, *56*, 1797.

(60) Prosser, G. A.; de Carvalho, L. P. S. Kinetic mechanism and inhibition of *Mycobacterium tuberculosis* D-alanine:D-alanine ligase by the antibiotic D-cycloserine. *FEBS Journal* **2013**, *280*, 1150–1166.

(61) Briffotiaux, J.; Liu, S.; Gicquel, B. Genome-Wide Transcriptional Responses of *Mycobacterium* to Antibiotics. *Front. Microbiol.* **2019**, *10*, 249 DOI: 10.3389/fmicb.2019.00249.

(62) Johnsson, K.; King, D. S.; Schultz, P. G. Studies on the Mechanism of Action of Isoniazid and Ethionamide in the Chemotherapy of Tuberculosis. *J. Am. Chem. Soc.* **1995**, *117*, 5009–5010.

(63) Milanes, C. L.; Pernalet, N.; Starosta, R.; Perez-Gonzalez, M.; Paz-Martinez, V.; Belloir-Font, E. Altered response of adenylate cyclase to parathyroid hormone during compensatory renal growth. *Kidney Int.* **1989**, *36*, 802–9.

(64) Bacon, J.; Alderwick, L. J.; Allnutt, J. A.; Gabasova, E.; Watson, R.; Hatch, K. A.; Clark, S. O.; Jeeves, R. E.; Marriott, A.; Rayner, E.; Tolley, H.; Pearson, G.; Hall, G.; Besra, G. S.; Wernisch, L.; Williams, A.; Marsh, P. D. Non-replicating *Mycobacterium tuberculosis* elicits a reduced infectivity profile with corresponding modifications to the cell wall and extracellular matrix. *PLoS One* **2014**, *9*, No. e87329.

(65) Rose, J. D.; Maddry, J. A.; Comber, R. N.; Suling, W. J.; Wilson, L. N.; Reynolds, R. C. Synthesis and biological evaluation of trehalose

analogs as potential inhibitors of mycobacterial cell wall biosynthesis. *Carbohydr. Res.* **2002**, *337*, 105–120.

(66) Barry, C. S.; Backus, K. M.; Barry, C. E.; Davis, B. G. ESI-MS Assay of *M. tuberculosis* Cell Wall Antigen 85 Enzymes Permits Substrate Profiling and Design of a Mechanism-Based Inhibitor. *J. Am. Chem. Soc.* **2011**, *133*, 13232–13235.

(67) Viljoen, A.; Richard, M.; Nguyen, P. C.; Fourquet, P.; Camoin, L.; Paudal, R. R.; Gnawali, G. R.; Spilling, C. D.; Cavalier, J.-F.; Canaan, S.; Blaise, M.; Kremer, L. Cyclopostins and cyclophostin analogs inhibit the antigen 85C from *Mycobacterium tuberculosis* both *in vitro* and *in vivo*. *J. Biol. Chem.* **2018**, *293*, 2755–2769.

(68) Crespo, M.; Martinez, M.; de Pablo, E. Activation volumes for intramolecular oxidative C–X (X = H, F, Cl or Br) addition to platinum(II) imine complexes as a proof of the intimate mechanism. *J. Chem. Soc., Dalton Trans.* **1997**, 1231–1236.

(69) Clark, P. W.; Dyke, S. F.; Smith, G.; Kennard, C. H. L. The cyclopalladation of benzyldenebenzylamines. *J. Organomet. Chem.* **1987**, *330*, 447–460.

(70) Anderson, C. M.; Crespo, M.; Kfoury, N.; Weinstein, M. A.; Tanski, J. M. Regioselective C–H Activation Preceded by  $\text{C}_{\text{sp}^2}$ – $\text{C}_{\text{sp}^3}$  Reductive Elimination from Cyclometalated Platinum(IV) Complexes. *Organometallics* **2013**, *32*, 4199–4207.

(71) Zhang, T.; Li, S.-Y.; Nuernberger, E. L. Autoluminescent *Mycobacterium tuberculosis* for Rapid, Real-Time, Non-Invasive Assessment of Drug and Vaccine Efficacy. *PLoS One* **2012**, *7*, No. e29774.

(72) Liu, Y.; Gao, Y.; Liu, J.; Tan, Y.; Liu, Z.; Chhotaray, C.; Jiang, H.; Lu, Z.; Chivala, G.; Wang, S.; Makafe, G.; Islam, M. M.; Hameed, H. M. A.; Cai, X.; Wang, C.; Li, X.; Tan, S.; Zhang, T. The compound TB47 is highly bactericidal against *Mycobacterium ulcerans* in a Buruli ulcer mouse model. *Nat. Commun.* **2019**, *10*, 524.

(73) Nateche, F.; Martin, A.; Baraka, S.; Palomino, J. C.; Khaled, S.; Portals, F. Application of the resazurin microtitre assay for detection of multidrug resistance in *Mycobacterium tuberculosis* in Algiers. *J. Med. Microbiol.* **2006**, *55*, 857–860.

(74) Mosaei, H.; Molodtsov, V.; Kepplinger, B.; Harbottle, J.; Moon, C. W.; Jeeves, R. E.; Ceccaroni, L.; Shin, Y.; Morton-Laing, S.; Marrs, E. C. L.; Wills, C.; Clegg, W.; Yuzenkova, Y.; Perry, J. D.; Bacon, J.; Errington, J.; Allenby, N. E. E.; Hall, M. J.; Murakami, K. S.; Zenkin, N. Mode of Action of Kanglemycin A, an Ansamycin Natural Product that Is Active against Rifampicin-Resistant *Mycobacterium tuberculosis*. *Mol. Cell* **2018**, *72*, 263–274.e5.

(75) James, B. W.; Williams, A.; Marsh, P. D. The physiology and pathogenicity of *Mycobacterium tuberculosis* grown under controlled conditions in a defined medium. *J. Appl. Microbiol.* **2000**, *88*, 669–77.

(76) Lambert, R. J. W. Susceptibility testing: inoculum size dependency of inhibition using the Colworth MIC technique. *J. Appl. Microbiol.* **2000**, *89*, 275–279.

(77) Lambert, R. J.; Pearson, J. Susceptibility testing: accurate and reproducible minimum inhibitory concentration (MIC) and non-inhibitory concentration (NIC) values. *J. Appl. Microbiol.* **2000**, *88*, 784–90.

(78) Luo, S.; Pal, D.; Shah, S. J.; Kwatra, D.; Paturi, K. D.; Mitra, A. K. Effect of HEPES Buffer on the Uptake and Transport of P-Glycoprotein Substrates and Large Neutral Amino Acids. *Mol. Pharmacol.* **2010**, *7*, 412–420.

(79) Borgers, K.; Ou, J. Y.; Zheng, P. X.; Tiels, P.; Van Hecke, A.; Plets, E.; Michielsen, G.; Festjens, N.; Callewaert, N.; Lin, Y. C. Reference genome and comparative genome analysis for the WHO reference strain for *Mycobacterium bovis* BCG Danish, the present tuberculosis vaccine. *BMC Genomics* **2019**, *20*, 561.

(80) Kapopoulou, A.; Lew, J. M.; Cole, S. T. The MycoBrowser portal: A comprehensive and manually annotated resource for mycobacterial genomes. *Tuberculosis* **2011**, *91*, 8–13.

(81) Abrahams, K. A.; Cox, J. A. G.; Fütterer, K.; Rullas, J.; Ortega-Muro, F.; Loman, N. J.; Moynihan, P. J.; Pérez-Herrán, E.; Jiménez, E.; Esquivias, J.; Barros, D.; Ballell, L.; Alemparte, C.; Besra, G. S. Inhibiting mycobacterial tryptophan synthase by targeting the inter-subunit interface. *Sci. Rep.* **2017**, *7*, 9430.

- (82) Briffotiaux, J.; Huang, W.; Wang, X.; Gicquel, B. MmpS5/MmpL5 as an efflux pump in *Mycobacterium* species. *Tuberculosis* **2017**, *107*, 13–19.
- (83) Abrahams, K. A.; Cox, J. A. G.; Spivey, V. L.; Loman, N. J.; Pallen, M. J.; Constantinidou, C.; Fernández, R.; Alemparte, C.; Remuiñán, M. J.; Barros, D.; Ballell, L.; Besra, G. S. Identification of Novel Imidazo[1,2-a]pyridine Inhibitors Targeting *M. tuberculosis* QcrB. *PLoS One* **2012**, *7*, No. e52951.
- (84) Gupta, R. S.; Lo, B.; Son, J. Phylogenomics and Comparative Genomic Studies Robustly Support Division of the Genus *Mycobacterium* into an Emended Genus *Mycobacterium* and Four Novel Genera. *Front. Microbiol.* **2018**, *9*, 67.
- (85) Neagoie, C. D.; Peng, X.; Tortorella, M. D.; Fossey, J. S.; Alderwick, L. J.; Feula, A.; Yoshizawa, A.. Preparation of antibacterial compounds: WO2020206594 A1 2020, 10–15.